NACA

RESEARCH MEMORANDUM

A PRESSURE-DISTRIBUTION INVESTIGATION OF A SUPERSONIC AIRCRAFT FUSELAGE AND CALIBRATION OF THE MACH NUMBER 1.59 NOZZLE OF THE LANGLEY 4- BY 4-FOOT SUPERSONIC TUNNEL

By

Morton Cooper, Norman F. Smith, and Julian H. Kainer

Langley Aeronautical Laboratory
Langley Air Force Base, Va.

NATIONAL ADVISORY COMMITTEE FOR AERONAUTICS

WASHINGTON

July 29, 1949

Classification cancelled (or changed to UNCLASSIFIED)

By Authority of NASA Tech. Pub. Announcement #12

(OFFICER AUTHORIZED TO CHANGE)

By 2d Maj F.J.

NAME AND

AMB

GRADE OF OFFICER MAKING CHANGE)

3 Apr 61

DATE

NACA RM L9E27a

[redacted]

NATIONAL ADVISORY COMMITTEE FOR AERONAUTICS

RESEARCH MEMORANDUM

A PRESSURE-DISTRIBUTION INVESTIGATION OF A SUPERSONIC-AIRCRAFT FUSELAGE AND CALIBRATION OF THE MACH NUMBER 1.59 NOZZLE OF THE LANGLEY 4- BY 4-FOOT SUPERSONIC TUNNEL

By Morton Cooper, Norman F. Smith, and Julian H. Kainer

SUMMARY

Pressure-distribution tests of a supersonic-aircraft fuselage with and without canopies (body of revolution without canopies) have been conducted in the Langley 4- by 4-foot supersonic tunnel at a Mach number of 1.59 and a Reynolds number of 2.60×10^6. These data were obtained upon completion of a series of calibration tests of the nozzle at a Mach number of 1.59. The results of the calibration tests indicated that the flow properties in the test section have a relatively high degree of uniformity and are suitable for aerodynamic testing.

For the fuselage without canopies (body of revolution), good agreement between experiment and theory was indicated at small angles of attack. At the higher angles of attack, the maximum discrepancies occurred in the vicinity of the fuselage side ($\phi = 90^\circ$).

For the complete fuselage configuration (with canopies), a localized positive pressure peak existed over the windshield. This peak, together with the remainder of the pressures on the upper surface of the canopy, can be estimated with sufficient accuracy for most structural design purposes.

INTRODUCTION

With the advent of supersonic flight by piloted aircraft, an immediate need exists for data applicable to aircraft designed for supersonic operation. Consequently, a pressure-distribution investigation of a large model of a fuselage of a sweptback-wing airplane has been conducted in the Langley 4- by 4-foot supersonic tunnel. The test model was selected to represent a supersonic-aircraft configuration in order that fundamental data having immediate practical interest would

[redacted]

be obtained. Since the basic fuselage without canopies is a body of revolution, these experimental results are applicable for missile configurations as well.

This paper presents the pressure measurements over the fuselage with and without canopies at a Mach number of 1.59 and at a Reynolds number of 2.60×10^6. In addition, comparisons of the experimental results with theoretical calculations are presented.

This paper contains a brief description of the Langley 4- by 4-foot supersonic tunnel and somewhat detailed calibration data to serve as a reference for future papers.

SYMBOLS

Free-stream conditions:

ρ	mass density of air
V	airspeed
a	speed of sound in air
M	Mach number (V/a)
β	Mach angle $\left(\sin^{-1}\frac{1}{M}\right)$
q	dynamic pressure $\left(\frac{1}{2}\rho V^2\right)$
p	static pressure

Fuselage geometry:

α	angle of attack of fuselage center line measured in plane of symmetry of airplane
ϕ	fuselage polar angle, degrees (0° at bottom)

Air-stream geometry:

θ_H	angle between tunnel center line and flow direction measured in a horizontal plane (positive to right when viewed looking upstream, fig. 2)

θ_V angle between tunnel center line and flow direction measured in a vertical plane (positive for upflow, fig. 2)

Pressure data:

p_l local static pressure

P pressure coefficient $\left(\frac{p_l - p}{q}\right)$

LANGLEY 4- BY 4-FOOT SUPERSONIC TUNNEL

General Description

The Langley 4- by 4-foot supersonic tunnel is a rectangular, closed-throat, single-return wind tunnel (fig. 1) driven by a seven-stage axial-flow compressor. The compressor has a design maximum compression ratio of 2 and volume flow of 870,000 cubic feet per minute. The tunnel has been designed for a nominal Mach number range from 1.2 to 2.2 and is powered by a 6000-horsepower electric-drive system. With the present power, the stagnation pressure is limited to approximately 0.3 atmosphere. The nominal operating stagnation temperature is 110° F with controls available to maintain any temperature in a range from about 85° F to 140° F. The cooling coils are located diagonally in the corner downstream from the compressor. The tunnel air is dried prior to and during tests by passage through an external drying circuit consisting of a circulating pump and an activated alumina dryer. The dryer is capable of reducing the stagnation dew point to about -60° F. It has been found in practice, however, that the present leak rate of the tunnel (equivalent to a $\frac{1}{8}$-inch-diameter hole), coupled with the relatively small dryer capacity, establishes a practical lower limit of about -35° F. Seal-off doors are provided in the tunnel passage to isolate the test section during model changes.

At the present time, the tunnel is in a transitory state with repowering installations in progress to increase the tunnel power to 45,000 horsepower. This will result essentially in an increase in tunnel stagnation pressure from the present limit of 0.3 atmosphere to approximately 2.0 atmospheres with corresponding increases in test Reynolds numbers.

Supersonic Nozzle and Test Section

General description.— The tunnel has a rectangular nozzle and test section (fig. 1) consisting of two fixed parallel side walls and two horizontal flexible nozzle walls; the side walls and nozzle walls are 25 feet long and are continuous from a point 66 inches upstream of the throat to the end of the test section (fig. 2). For the existing Mach number 1.59 nozzle, the test section has a width of 4.5 feet, a height of 4.4 feet, and a length of uniform-flow region along the wall of approximately 7 feet.

The supersonic nozzle and test section are formed by deflecting the horizontal flexible walls against a series of fixed interchangeable templates which have been designed to produce uniform flow in the test section. The deflection of the nozzle walls, which are 0.465 inch thick, is accomplished by means of a series of jacking screws attached to transverse corrugations on the outside of the flexible walls. These corrugations, which are fastened to the flexible walls by means of studs welded to the under side of the plate, serve to increase the transverse stiffness of the nozzle plate and to distribute the jacking loads, thereby minimizing local wall irregularities. For this series of tests, temporary mild steel nozzle plates were used in place of the permanent set of machined and polished stainless-steel plates. Though these temporary plates were not machined and did contain some extremely small periodic waves caused by the corrugation stud welding, the flow in the test section is relatively uniform and the effect of these waves appears small.

Aerodynamic design.— The nozzle for the Langley 4- by 4-foot supersonic tunnel was designed by the method of characteristics for a test-section Mach number of 1.606. In anticipation of the repowering, a boundary-layer correction for 1 atmosphere stagnation pressure was estimated by the method of reference 1. In applying this correction, the displacement thickness of the boundary layer was computed along the nozzle walls, and it was assumed that the same thickness existed along the side walls. The combined effect of both boundary layers was then arbitrarily applied to the ordinates computed by the method of characteristics to satisfy one-dimensional continuity relations. Since all the results presented in this paper were obtained at a stagnation pressure of 0.25 atmosphere, it should be expected that the test-section Mach number would be lower than the theoretical value of 1.606 because of the more rapid growth of the boundary layer at the lower pressures (lower Reynolds numbers). The magnitude of this decrease in Mach number was estimated from one-dimensional considerations as 0.012 at station 241. (See fig. 2. Station 241 is the main tunnel calibration station.) Since the effects of condensation at normal operating conditions are to further reduce the Mach number from the isentropic

value by an increment of the order of 0.003 (see section entitled "Test-Section Calibration"), the estimated theoretical Mach number of 1.59 for the actual operating conditions compares favorably with the measured tunnel Mach numbers.

Test-Section Calibration

A series of calibration tests were conducted to determine the Mach number and flow angularity distribution in the test section of the tunnel. In addition to establishing quantitatively these flow parameters, tests were undertaken to define the operating dew-point criteria for minimizing the adverse effects of condensation on the flow in the test section.

Apparatus.- The principal surveying instrument used during the calibration was a cruciform probe. (See figs. 3(a) and 3(b).) This probe consisted of four 5° wedges of rectangular plan form mounted radially with a 90° spacing about a circular cylinder having a conical nose. One surface of each wedge was in a plane containing the axis of the probe. A static-pressure orifice was located in the two-dimensional region of this surface of each wedge. This arrangement simulated two 0° wedges at right angles to each other. In addition, a total-pressure tube was mounted on the probe (fig. 3(a)) so that a total-pressure survey could be made simultaneously with the static-pressure measurements. From these five pressure readings, the flow angles, Mach number, and static pressure were calculated by the shock and expansion relations. During these surveys, a pitot-static probe (fig. 3(c)), which was designed on the basis of the calibration results presented in reference 2, was also used to establish and to check accurately the static pressure and Mach numbers as determined from the cruciform probe.

Tests.- The initial series of tests consisted of systematically varying the stagnation dew point, pressure, temperature, and compressor speed through the following ranges to establish the operating conditions of the tunnel:

Stagnation pressure, atmosphere	0.125 to 0.3
Stagnation dew point, °F	-36 to 40
Stagnation temperature, °F	85 to 140
Compressor speed, rpm	1200 to 1300

During these tests, static-pressure measurements were made throughout the nozzle and test section. After the stagnation operating conditions (pressure of 0.25 atmosphere, dew point of -35° F, and temperature of 110° F) were established, an axial survey (direction of the x-axis;

[redacted]

fig. 2) was made for these conditions. Data were obtained from the cruciform probe at 2-inch intervals in the test section from station 215 to station 298 (a length of 83 in.) at a distance 1 inch below the tunnel center line. In addition, a transverse survey (direction of the y-axis; fig. 2) was made simultaneously for three positions - $9\frac{3}{4}$ inches above, on, and $9\frac{3}{4}$ inches below the tunnel axis at station 241. (See fig. 2.)

Corrections.- During the axial calibration of the test section, it was found that the cruciform probe indicated an erroneously high static pressure, resulting in an indicated Mach number which was low by about 0.03. This Mach number decrement was believed to be caused by either the forward propagation of the positive interference pressures from the juncture of the wedges and the cylindrical central body, or the closeness of the orifices to the Mach lines from the corners of the measuring planes. Calibration of the probe through an angle-of-attack range of $\pm 1^{\circ}$, however, indicated that although the absolute static pressure was in error, the indicated variations in static pressure were correct to within 0.03° flow angle (within the experimental accuracy of the tests). In order to establish the absolute pressure and Mach number from the data obtained with the cruciform probe, it was necessary to use a pitot-static probe. (See fig. 3(c).) By comparing the static pressure and Mach number determined from both the pitot-static and cruciform probe at the same point in the tunnel, it was possible to establish the cruciform-probe instrument error and in this way determine the absolute Mach number and static-pressure variations in the tunnel. The accuracy of the results obtained from the pitot-static probe was further checked by individual static- and total-pressure probes and by measurements made on the surface of a cone. In addition, the mean value of the corrected static pressure, determined from an average of all the cruciform-probe data obtained throughout the axial survey, agreed, within experimental accuracy, with the average value of the wall static pressures obtained over a corresponding length of the test-section wall.

During the air-stream surveys, eight different cruciform probes were used, six simultaneously during the transverse surveys and two during the axial survey. The probe angles were accurately measured in the vicinity of the static orifices and it was found that there was, in general, a slight included angle between the parallel planes which was less than 0.5° in all cases. In order to facilitate the reduction of the data, it was convenient to use the basic shock-expansion relations computed for a 0° wedge and to apply a computed Mach number correction of 0.0023 per tenth of a degree included angle. Because of the small magnitude of the included angles and the linearity of the pressure as a function of angle in this range, there is no correction to the flow-angle variations indicated by the wedges.

During the axial survey, the geometric-probe angles were determined relative to the tunnel center line so that the flow angles could be established with this as a reference. In the transverse surveys, no geometric angles were measured. However, it was possible to establish the geometric-flow angles along the transverse survey on the y-axis (fig. 2) from the common point with the axial survey. For the vertical-flow angles (θ_V) $9\frac{3}{4}$ inches above and below the test-section axis (y-axis; fig. 2), it was possible to calculate the geometric angles on the vertical plane of symmetry (x-z plane; fig. 2) from the axial survey by assuming two-dimensional flow and constructing the characteristic net. The validity of this procedure was previously established by a comparison of the measured Mach numbers and horizontal-flow angles (θ_H) on the axial survey (along the x-x axis; fig. 2) with values computed from the transverse (y-y axis; fig. 2) survey. The agreement was good and was within the experimental accuracy of the tests. (See section entitled "Results and Discussion".) There is no apparent method from the data available for the accurate determination of the geometric horizontal-flow angles (θ_H) $9\frac{3}{4}$ inches above and below the tunnel center line. However, from installation considerations and a comparison of these data $\left(9\frac{3}{4}\text{ in. above and below tunnel center line}\right)$ with the tunnel-center-line data, it is probable that the angles of the probes relative to the tunnel center line were extremely small and the flow angles obtained directly from the probes were nearly equal to the geometric-flow angles relative to the tunnel center line.

From an analysis of the data obtained during the calibration tests, the probable errors in the measurement of the flow angles and Mach numbers were computed by the method of least squares and are as follows:

Absolute flow angles, degrees	± 0.1
Flow-angle variations, degrees	± 0.05
Mach number variations	± 0.003

Based on a comparison of the Mach number calculated from the pitot-static probe, individual static- and total-pressure tubes, wall static pressures and settling-chamber total pressure, and total-pressure readings in the test section and the settling chamber, it is estimated that the absolute value of the Mach number is accurate to within ± 0.01.

Results and discussion.- A representative phase of the results of the dew-point investigation is presented in figure 4. In this figure, the wall-pressure data have been presented in terms of indicated Mach number (based on isentropic total pressure) as a function of

[redacted]

stagnation dew point at four representative wall stations along the test section for the range of compressor speeds for supersonic flow. Though the indicated Mach numbers are in error when condensation occurs (the actual Mach numbers will be lower because of the loss in total pressure due to condensation), they show the pronounced importance of the dew point on affecting the flow in the test section. The large decrease in indicated Mach number from a value of about 1.60 at a dew point of -36° F to about 1.44 at 40° F is shown. Based on the results of these tests, coupled with additional measurements in the free stream, it was concluded that all tests should be conducted at a dew point of or below -35° F. Even at -35° F, there is a loss of one-half of 1 percent in total pressure which can be directly attributed to condensation since tests at still lower dew points eliminate this loss in total pressure. The necessity for operating at such low dew points is a consequence of the low stagnation pressures. With a dew point of -35° F, the specific humidity is relatively high, 0.00043 (pounds of water vapor per pound of dry air) for a stagnation pressure of 0.25 atmosphere.

Figure 5 presents an illustrative wall-indicated Mach number distribution measured on the center line of the upper- and lower-surface nozzle wall for representative operating conditions. The theoretical curve for the supersonic region was obtained from the characteristic calculations; whereas the curve for the subsonic region was obtained from one-dimensional isentropic-flow relations. This procedure for the subsonic region appears justified because of the relatively low rate of change of cross-sectional area with distance in the vicinity of the throat. The data from the upper and lower surface both agree reasonably well with the theoretical distribution, but individually indicate a small systematic asymmetry between the upper and lower surfaces. Because of the temporary nature of these nozzle plates and the relatively good quality of the flow in the test section, no attempts have been made to modify the nozzle contour. In an arbitrary length equal to the height of the test section, the maximum variation in Mach number along the wall is ± 0.007.

The basic results of the axial survey are presented in figure 6 for stagnation conditions of 0.25 atmosphere, 110° F, and a dew point of -35° F. In order to indicate clearly the reproducibility of the data, repeat tests are designated by flagged symbols. In addition, since the axial survey was conducted in two separate intervals, (stations 215 to 243.5 and stations 242.5 to 298) different symbols have been used for each interval.

In order to indicate the accuracy with which the data from the transverse survey could be used for computing the axial survey, a representative set of horizontal-flow angles (θ_H) computed from the transverse survey are shown in figure 6 together with the experimental

data. As can be seen from this figure, the agreement between the computed and measured values is excellent.

In a discussion of the flow parameters in supersonic tunnels, some basic length for comparison must be assumed. Since, in general, the length of all models must be less than the height of the tunnel times the cotangent of the Mach angle, this fundamental length (5.5 ft at $M = 1.59$ for the Langley 4- by 4-foot supersonic tunnel) together with the present model length (2.5 ft) have been used for reference dimensions. The significant variations of the flow parameters as obtained from the longitudinal survey (fig. 6) are summarized in the following table:

Item	Test-section height × cot β	Model length
Interval	Stations 215 to 281	Stations 235 to 265
Maximum Mach number range	1.585 to 1.604	1.585 to 1.595
Maximum-horizontal-flow-angle (θ_H) range	−0.05 to 0.20	0 to 0.20
Maximum-vertical-flow-angle (θ_V) range	−0.15 to 0.30	0 to 0.30
Maximum-pressure-coefficient range	−0.012 to 0.004	−0.005 to 0.004

Since the present model installation provides for angle-of-attack variations in a horizontal plane, Mach number variations in the position of representative wing locations have been computed from the axial survey. In the region of the wings for the first complete model installation, the variation in Mach number is ±0.01 and takes place in a length of 26 inches (13 in. above and below the tunnel axis).

The results of the data obtained from the transverse survey at station 241 are shown in figures 7 to 9 and are summarized for a length of 26 inches in the following table:

Item \ Location	$9\frac{3}{4}$ inches above tunnel center line	On tunnel center line	$9\frac{3}{4}$ inches below tunnel center line
Maximum Mach number range	1.595 to 1.601	1.581 to 1.591	1.591 to 1.597
Maximum-horizontal-flow-angle (θ_H) range	[a]−0.13 to 0.05	−0.03 to 0.22	[a]−0.05 to 0.15
Maximum-vertical-flow-angle (θ_V) range	−0.25 to 0.10	−0.06 to 0.20	0 to 0.18

[a]Incremental values.

On the basis of the data of figures 6 to 9 and the tabulated values presented herein, the general-flow properties in the test section are considered to have a relatively high degree of uniformity, and are suitable for aerodynamic testing.

MODEL AND INSTALLATION

The test model was constructed from steel to coordinates presented in table I and is shown in figure 10. The basic model (without canopies) is a body of revolution having an over-all length of 30.267 inches and a fineness ratio of 9.4 without canopies. The top and bottom canopies are removable so that the fuselage can be tested as a body of revolution. The aft part of the fuselage is integral with the supporting sting. During the initial phases of the test program, the supporting sting had a 10° cone angle beginning essentially at the rear of the model. The sting was modified during the test program to approximately a 3° cone angle (fig. 10), the equivalent of a constant-stress condition for the first 4 inches of the sting. The pressure orifices were located at various radial positions at nine basic stations of the model as shown in figure 10. In addition, one comprehensive longitudinal row of orifices was located along the upper surface ($\phi = 180°$) of the basic body (no canopies). For the fuselage with canopies installed, the orifices located at approximately 150° were moved to the canopy juncture. The pressures were photographically recorded from multiple-tube manometers filled with Alkazene 42. This manometer fluid, having a specific gravity of approximately 1.75, was found particularly suited for these tests because of its extremely low vapor pressure and low viscosity.

The installation of the body of revolution in the tunnel is shown in figure 11. A scale drawing of the installation showing principal dimensions is presented in figure 12. The angle of attack was varied in a horizontal plane through fixed increments by rotating the model about the 59-percent position of the fuselage.

TESTS, CORRECTIONS, AND ACCURACY

Tests

The basic pressure data were obtained for the fuselage as a body of revolution and with canopies for an angle-of-attack range from -5° to 10° at a Mach number of 1.59 and a Reynolds number of 2.60×10^6 based on the fuselage length. This Reynolds number and Mach number condition corresponds to full-scale similarity at an altitude of 116,000 feet. The aerodynamic data were obtained at tunnel-stagnation conditions of: Dew point, -35° F; pressure, 0.25 atmosphere; and temperature, 110° F.

Corrections and Accuracy

Since the magnitude of the flow angle, Mach number, and pressure-coefficient gradients are small in the vicinity of the model, no corrections have been applied to the data. It is estimated that the accuracy of the data is as follows:

Mach number	±0.01
Angle of attack:	
Geometric measurement (probable error)	±0.02
Maximum flow irregularity	$\begin{cases}+0 \\ -0.20\end{cases}$
Angle of yaw:	
Maximum flow irregularity	$\begin{cases}+0.30 \\ -0\end{cases}$
Absolute pressure coefficient	±0.010
Variation of radial pressure coefficient	±0.005

PRESENTATION OF RESULTS

The basic data obtained during the pressure tests of the fuselage as a body of revolution and with canopies are presented in figures 13 and 14, respectively, as a function of radial location for nine representative stations along the fuselage. The actual data presented in all

the figures have been tabulated in tables II to IV with additional data obtained during these tests but not used in analysis tabulated in tables V to VII. Where two columns are listed for a given angle, the data in the first column indicate the original sting configuration and the data in the second column indicate the modified-sting configuration. In order to prevent considerable overlapping of data, a large portion of the modified-sting data was not presented in figures 13 and 14. In all cases, however, the data omitted agree within about 0.007 in pressure coefficient with the data presented. All the data indicated in the figures by flagged symbols have been obtained with the modified-sting configuration. In order to compare the fuselage data with available theoretical calculations, the data for the fuselage as a body of revolution have been replotted in figure 15 as a function of the product of the angle of attack and the cosine of the radial angle ($\alpha \cos \phi$). At each station along the body, a comparison has been presented with the linearized theoretical results of Von Kármán and Moore (reference 3) and Tsien (reference 4). In this comparison, the linearized pressure coefficient has been defined as minus twice the axial perturbation velocity expressed in terms of the free-stream velocity. No theoretical results have been presented for station 46.2 because of the location of this station at a region of discontinuity of slope of the fuselage profile. No comparison is presented for station 93.5 because of the limited amount of data available and because of the probability of the sting materially affecting the results at this station. In addition, the theoretical nonlinear results for flow about a cone have been obtained from reference 5 for zero angle of attack and reference 6 for angle of attack and are included for station 5.6. Figure 16 compares the experimental axial pressures over the body of revolution for zero angle of attack with the linearized results of reference 3 and the nonlinear results obtained by the method outlined by Ferri (reference 7). For the present comparison, the effects of the shock curvature at zero angle of attack were estimated to be very small and hence neglected. A comparison of the experimental and linearized theoretical pressures over the upper surface of the body of revolution at angles of attack is presented in figure 17. Figure 18 presents a comparison of the pressure distribution over the upper surface of the canopy at zero angle of attack with two approximations for estimating these pressures. A limited amount of the experimental pressure data over the upper canopy for a range of angles of attack is presented in figure 19.

DISCUSSION

A direct comparison of the experimental data with the linearized theories of reference 3 and reference 4 can be made from an examination of figure 15; in addition, a semiquantitative comparison with all

available nonlinear theories for bodies of revolution at small angles of attack is also evident. This generalized comparison results from the fact that such inviscid nonlinear theories as those of Ferrari (reference 8), Stone (reference 9), and Ferri (reference 10) all investigate the problem from a viewpoint of considering the effects of a superposition of small perturbations of yaw velocities on the basic-zero-yaw configuration. In essence, the basic-spherical-coordinate velocities are represented by Fourier series of the form (see reference 6)

$$u = \bar{u} + \alpha \sum_{n=0}^{\infty} x_n \cos n\phi$$

$$v = \bar{v} + \alpha \sum_{n=0}^{\infty} y_n \cos n\phi$$

and

$$w = \alpha \sum_{n=0}^{\infty} z_n \sin n\phi$$

where the barred quantities indicate the zero yaw condition and the unbarred quantities represent the yawed condition. Since in each analysis, terms of the order of α^2 and higher are neglected, it is shown (reference 9) that, for the solution to be compatible with the boundary conditions, the Fourier coefficients for u, v, and w must be zero for $n \neq 1$ and the equations reduce to

$$u = \bar{u} + \alpha x_1 \cos \phi$$

$$v = \bar{v} + \alpha y_1 \cos \phi$$

$$w = \alpha z_1 \sin \phi$$

With the velocities expressed in this form, it is possible to obtain a similar form for the pressure-coefficient variation (reference 9):

$$P = \bar{P} + \Delta P \alpha \cos \phi$$

[redacted]

where ΔP depends solely on the body geometry and the free-stream Mach number. Though this discussion applies rigorously in the case of yawed cones where the shock curvature is zero (station 5.6), it is equivalent to neglecting the shock curvature in the method of Ferri (reference 10). If the effects of shock curvature are considered, then the quantity ΔP must depend, to some degree, on the angle of attack. This dependence would result in a separate straight line (fig. 15) for each angle of attack with the inclination of each line rotating about the pressure coefficient at $\alpha \cos \phi = 0$. For the Mach number and the angles of attack of this investigation, the effect of the shock curvature on the comparison of the pressures is small. It is estimated that this effect is exactly zero for the first three stations and the linearity of the pressure data presented in figure 15 shows a direct comparison with the theory of reference 10 for stations 5.6, 11.0, and 22.0. For the lower angles of attack, the comparison is again directly applicable to station 34.6. For the highest angles, small effects of shock curvature may be present. From an examination of figures 15(a) and 15(b) it can be seen that, in general, good agreement exists over the upper and lower surfaces (extremities of the curves), and the maximum discrepancy between experiment and theory occurs at $\phi = 90^\circ$ ($\alpha \cos \phi = 0$). Since the theoretical pressure at this location throughout the body is independent of shock-curvature effects, then the disagreement of each experimental curve with the theory in this vicinity must be a direct indication of the effects of the higher-order terms of the angle of attack. (It should be noted that the vertical shift of the linear-theory curves at $\alpha \cos \phi = 0$ to account for nonlinear considerations can be easily determined from fig. 16). Furthermore, since shock-curvature effects can only correspond to variations in slopes of the theoretical curves, the curved nature of the experimental trends must again be the effects of the higher-order terms of the angle of attack. Therefore, it is concluded that the shock-curvature terms are of secondary importance to the angle-of-attack terms in affecting the pressure-coefficient comparison presented in figure 15. If, however, any considerations of lift and moments are made, then the shock curvature may be of greater significance since these quantities depend directly on ΔP.

In general, relatively good agreement exists (fig. 15) between the experimental and theoretical results throughout the body length for small angles. As noted previously, the agreement is best on both the top ($\phi = 180^\circ$) and the bottom ($\phi = 0^\circ$) surfaces. At station 5.6, though the agreement with the theories of references 3, 4, 9, and 11 is good for the low angles of attack, the disagreement becomes quite pronounced, as might be expected, at the highest angle of attack, 10°. Though no calculations have been made to determine the angle for shock detachment, it can be readily reasoned that the shock remained attached throughout the angle-of-attack range and that discrepancies between the experimental and theoretical results again indicate the limitations of

the theory. As might be expected, the discrepancies between the theory and experiment begin at lower angles of attack as the rear of the body is approached. Towards the midsection and the rear of the body, the radial pressure variation is extremely small for low angles of attack, and the exact nature is beyond the precision of the tests. It is interesting to note that after approximately the 45-percent-fuselage station, the radial pressure distributions resemble much more closely the shape to be expected from an infinitely long, yawed, circular cylinder.

Though only a limited amount of data are available at the 93.5 percent station, there appears to be a significant effect of the original sting on the last-station data for angles of attack of 2° and 4° but which disappears at 5° and above. This discrepancy can be associated with the original sting since reducing the sting angle resulted in a decrease in the compression over the sting and hence a reduction in the pressures over the extreme rear of the body.

A more graphic visualization of the flow over the fuselage can be seen from figure 16 for zero angle of attack and over the upper surface ($\phi = 180^\circ$) of the fuselage for other angles from figure 17. The close agreement between the linear and nonlinear theories for the body at zero angle of attack would be expected in this Mach number range as shown for the conical nose by the calculations presented in reference 11. Though slightly better agreement is shown between the experimental data and the nonlinear theory, good agreement exists between both the linear and nonlinear theories and the experimental data for zero angle of attack up to about station 85. Beyond this point, the linearized theory indicates a rapid expansion; whereas the experimental data indicate a small axially symmetric separated region at the rear of the body. This separated region is quite probably caused by or materially influenced by the sting support. In comparing the experimental and theoretical curves, it should be noted that the surface slopes in the region between station 8.2 to station 20.9 and station 86.9 to station 100 were graphically determined from faired curves and, as such, the theoretical trends are considered more significant than the explicit values presented. For angles of attack up to 6°, the agreement between the linearized calculations and the experimental data remains good (fig. 17). At the last station there appears to be a slight sting effect for 4° and a somewhat larger effect for 2°. It should also be noted that good agreement exists for the upper surface at -5° angle of attack (under surface for 5°). For 10° angle of attack, the flow over the upper surface at the rear of the body is at a much lower pressure than indicated by theory. It is quite probable that the flow is separated and influenced to a large degree by the under-surface pressure. Since the flow over the body at positive angles of attack is of a spiral nature from the lower surface at the front to the upper surface at the rear, it is possible that the

boundary layer accumulates at the rear of the upper surface and separates. Since the lower surface would have very low pressures at the rear (see, for example, the -5° curve), these low pressures on the under surface could be transmitted to the upper surface through the separated boundary layer.

A comparison of the fuselage data with and without canopies (figs. 13, 14, 16, 17, 18, and 19) indicates expected trends. From a comparison of the curves of figures 13 and 14, it can be seen that there is no effect of the canopies on station 5.6; at station 10.9, the effect of the upper-surface canopy is to change markedly the pressures over the fuselage between radial locations of 90° and 180° with a high positive-pressure peak resulting on the abrupt increase in slope along the canopy windshield. At station 22.0, the effect of the canopies (both upper and lower) is felt on the pressures over the entire station though not to a very large degree between 0° and 60°. This, however, is just a coincidence for this particular configuration. Further rearward, there are no pronounced changes in pressures for the canopy configuration. This probably can be seen more clearly for the upper surface for zero angle of attack from figures 16 and 18 and for an angle of attack from figures 17 and 19.

In order to estimate the pressures over canopies and other protuberances for structural design of these components, two approximations were made which predicted the distribution over the upper surface of the upper canopy for zero angle of attack surprisingly well. In presenting these results, it is realized that there is no rigorous basis to expect agreement between the calculation and the data. From physical considerations, however, it appears that the two approximations would be expected to combine to give a reasonable result in many practical applications. In order to calculate the flow over the upper surface of the canopy for zero angle of attack, the fuselage was assumed to be a body of revolution with the canopy extending completely around the body. The pressure distribution was then calculated by the method of reference 3 and the results (method 1, fig. 18) show fairly good agreement with the experimental pressures except in the region of the canopy windshield. The overestimation of the pressure in this region by this method should be expected. The magnitude of the peak pressure on the canopy windshield was then estimated by assuming the windshield to be a body of revolution about the fuselage element intersecting the windshield in the 180° radial location. Using the Mach number of the flow over the region ahead of the canopy, the pressure on the windshield was determined from linearized-cone calculations and is shown as method 2 in figure 18. The agreement with the observed pressure is good. Hence by a combination of the two methods, the pressures over the top of the canopy can be estimated for most structural-design purposes.

CONCLUSIONS

Pressure-distribution tests of a supersonic-aircraft fuselage with and without canopies (body of revolution without canopies) have been conducted in the Langley 4- by 4-foot supersonic tunnel at a Mach number of 1.59 and a Reynolds number of 2.60×10^6. These data were obtained upon completion of a series of calibration tests of the nozzle at a Mach number of 1.59. The results of the calibration and pressure-distribution tests indicate the following conclusions:

1. The general-flow properties in the test section are considered to have a relatively high degree of uniformity and are suitable for aerodynamic testing.

2. For the fuselage without canopies (body of revolution), good agreement of the experimental data with both linear and nonlinear theoretical calculations was obtained at zero angle of attack up to 85 to 90 percent of the fuselage length. At distances greater than 90 percent, a generalized conclusion was not possible because of separation which was caused or aided by the sting.

3. A similar comparison for angles of attack up to 6° indicates that the axial agreement between the experimental data and the linearized theory remained good over both the upper ($\phi = 180^\circ$) and the lower ($\phi = 0^\circ$) surfaces.

4. The theoretical variation of pressure coefficient with $\alpha \cos \phi$ (a parameter used in computing the pressures around bodies of revolution at small angles of attack) agrees reasonably well with the experimental data. However, small but measurable discrepancies (occurring principally on the side of the body, $\phi = 90^\circ$) which increase with angle of attack were observed. These discrepancies indicate the relative importance of the squares and higher-order terms of the angle of attack and the viscous terms which are neglected in all theories presently available for small angles of attack.

5. For the complete fuselage configuration (with canopies), a localized positive-pressure peak existed over the windshield. This peak, together with the remainder of the pressures on the upper surface ($\phi = 180^\circ$) of the canopy, can be estimated with sufficient accuracy for most structural-design purposes.

Langley Aeronautical Laboratory
National Advisory Committee for Aeronautics
Langley Air Force Base, Va.

[redacted]

REFERENCES

1. Tetervin, Neal: Approximate Formulas for the Computation of Turbulent Boundary-Layer Momentum Thicknesses in Compressible Flows. NACA ACR L6A22, 1946.

2. Hasel, Lowell E., and Coletti, Donald E.: Investigation of Two Pitot-Static Tubes at Supersonic Speeds. NACA RM L8I02, 1948.

3. Von Kármán, Theodore, and Moore, Norton B.: Resistance of Slender Bodies Moving with Supersonic Velocities, with Special Reference to Projectiles. Trans. A.S.M.E., vol. 54, no. 23, Dec. 15, 1932, pp. 303-310.

4. Tsien, Hsue-Shen: Supersonic Flow over an Inclined Body of Revolution. Jour. Aero. Sci., vol. 5, no. 12, Oct. 1938, pp. 480-483.

5. Staff of the Computing Section, Center of Analysis (Under Direction of Zdeněk Kopal): Tables of Supersonic Flow around Cones. Tech. Rep. 1, M.I.T., 1947.

6. Staff of the Computing Section, Center of Analysis (Under Direction of Zdeněk Kopal): Tables of Supersonic Flow around Yawing Cones. Tech. Rep. 3, M.I.T., 1947.

7. Ferri, Antonio: Application of the Method of Characteristics to Supersonic Rotational Flow. NACA Rep. 841, 1946.

8. Ferrari, C.: Determination of the Pressure Exerted on Solid Bodies of Revolution with Pointed Noses Placed Obliquely in a Stream of Compressible Fluid at Supersonic Velocity. R.T.P. Translation No. 1105, British Ministry of Aircraft Production. (From Atti R. Accad. Sci. Torino, vol. 72, Nov.-Dec. 1936, pp. 140-163.)

9. Stone, A. H.: On Supersonic Flow past a Slightly Yawing Cone. Jour. Math. and Phys., vol. XXVII, no. 1, April 1948, pp. 67-81.

10. Ferri, Antonio: The Methods of Characteristics for the Determination of Supersonic Flow over Bodies of Revolution at Small Angles of Attack. NACA TN 1809, 1949.

11. Taylor, G. I., and Maccoll, J. W.: The Air Pressure on a Cone Moving at High Speeds. Proc. Roy. Soc. (London), ser. A, vol. 139, no. 838, Feb. 1, 1933, pp. 278-311.

TABLE I.- FUSELAGE AND CANOPY [illegible] COORDINATES

(See fig. 10)

Streamline body (in.)	
Station	Radius
0	0
2.480	.638
3.396	.852
4.262	1.030
5.134	1.174
5.778	1.252
6.328	1.290
11.800	1.517
12.172	1.532
13.952	1.606
22.020	1.606
23.374	1.549
23.644	1.538
24.310	1.510
24.976	1.482
25.308	1.468
25.782	1.448
26.308	1.426
27.025	1.385
27.640	1.350
28.972	1.186
30.267	.900

Top canopy (in.)

Station 2.964		Station 4.262		Station 5.128		Station 6.560		Stations 13.952 to 22.020	
x	y	x	y	x	y	x	y	x	y
0	0.872	0	1.432	0	1.814	0	2.030	0	2.032
.126	.800	.132	1.408	.132	1.794	.132	2.016	.266	1.964
.214	.722	.266	1.320	.266	1.736	.266	1.968	.392	1.864
		.400	1.180	.400	1.626	.400	1.882	.532	1.664
		.574	.856	.532	1.424	.532	1.722	.612	1.482
				.684	.956	.598	1.596		
						.666	1.376		
						.720	1.066		

Station 23.374		Station 23.644		Station 24.310		Station 24.976		Station 25.308		Station 25.782	
x	y	x	y	x	y	x	y	x	y	x	y
0	2.032	0	2.027	0	2.010	0	2.002	0	1.977	0	1.920
.256	1.964	.246	1.964	.352	1.864	.322	1.864	.304	1.856	.188	1.864
.378	1.864	.370	1.864	.460	1.664	.416	1.664	.388	1.664	.320	1.664
.503	1.664	.491	1.664	.500	1.482	.444	1.482	.404	1.482	.344	1.482
.570	1.440	.556	1.436	.505	1.424	.447	1.414	.405	1.411	.354	1.404

Bottom canopy (in.)

Station 5.994		Station 8.892		Stations 12.172 to 22.152		Station 24.310		Station 26.640	
x	y	x	y	x	y	x	y	x	y
0	1.398	0	1.788	0	2.080	0	1.878	0	1.510
.066	1.392	.066	1.784	.066	2.080	.132	1.854	.132	1.494
.132	1.372	.132	1.768	.132	2.076	.266	1.776	.266	1.416
.198	1.338	.198	1.736	.198	2.068	.400	1.584	.308	1.372
.266	1.282	.266	1.688	.266	2.028	.490	1.428		
.306	1.232	.334	1.614	.334	1.954				
		.400	1.472	.400	1.824				
		.462	1.316	.466	1.684				
				.550	1.508				

[redacted]

NACA

TABLE II.- PRESSURE-COEFFI[redacted]PRESENTED IN FIG. 13)

FOR THE FUSELAGE AS A BODY OF REVOLUTION

Station (percent)	Radial angle ø	Angle of attack											
		-5	-5	0	0	2	2	4	4	6	6	10	10
5.6	0	0.129	0.138	0.194	0.201	0.224		0.261		0.303		0.376	0.387
	60	.148		.198		.212		.225		.236		.240	.257
	90	.179		.200		.195		.192		.186		.137	.155
	120	.230		.200		.183		.166		.147		.080	.094
	180	.283		.200		.173		.148		.131		.078	
	180											.080	
10.9	0	.087		.146	.152	.179		.213		.246		.326	.332
	60	.107		.148		.161		.172		.181		.188	.196
	60					[a].174							
	90		.144	.156		.150		.148		.135	.135	.098	.106
	120	.187		.163	.158	.142		.131	.121	.104	.103	.056	.055
	180	.199	.213	.156		.126		.099	.089	.078	.064	.038	.033
22.0	0	-.085		-.056			-.039	-.017		.001	-.006	.050	.057
	60	-.085		-.052	-.057	-.054			-.043	-.042	-.037	-.038	-.034
	120	-.048		-.054		-.066			-.077	-.089	-.087	-.123	-.119
	147	-.022		-.052		-.068			-.083	-.087	-.091	-.102	-.111
	180	-.007		-.056		-.070		-.080		-.078		-.104	
	180											-.104	
34.6	0	-.028		-.018	-.015	-.011		.001		.019		.054	.059
	60	-.038		-.014		-.017			-.017	-.023		-.044	
	90	-.038		-.012		-.021			-.027	-.044		-.092	-.091
	120	-.022		-.012		-.021			-.029	-.042	-.041	-.080	-.077
	153	.001	.010	-.018	-.011	-.027	-.021	-.031	-.023	-.034	-.029	-.041	-.034
	180	.015		-.012		-.021		-.023		-.019		-.017	
46.2	0		[a]-.040			[a]-.041							
	90	-.069	-.063	-.041	-.047	-.050		-.048	-.055		-.071	-.121	-.125
	120	-.050		-.031	-.045	-.046		-.049	-.053		-.059	-.098	-.095
	158	-.032	-.013	-.047		-.050		-.049		-.050	-.037	-.062	-.040
	180	-.032	-.008	-.047		-.050		-.051		-.050	-.033	-.060	-.038
59.7	0	-.028	-.019	-.027		-.036	-.033	-.027		-.025	-.017	-.005	.005
	90	-.046	-.043	-.025	-.027	-.030		-.035		-.052	-.049	-.102	-.093
	120	-.039		-.022	-.031	-.030		-.031	-.035	-.052	-.049	-.086	-.081
	158	-.034	-.031	-.035		-.036	-.031	-.035		-.028		-.040	-.024
	180	-.024		-.035	-.031	-.034		-.031		-.021	-.025	-.009	-.012
73.1	0		-.043	-.058		-.062	-.057	-.056	-.051	-.046		-.035	-.028
	60	-.069		-.052	-.055	-.058		-.062		-.070		-.107	-.103
	90	-.081		-.056		-.062		-.072		-.091	-.087	-.117	-.113
	120	-.073		-.056		-.060		-.060		-.072		-.109	-.101
	158	-.052		-.056		-.054		-.053		-.042		-.072	-.069
	180	-.048		-.058		-.058		-.056	-.051	-.046		-.050	-.040
84.3	0	-.022		-.037	-.041	-.046		-.047		-.042		-.035	-.032
	60	-.048	-.043	-.043		-.048		-.049	-.053		-.067	-.096	-.093
	90	-.063	-.057	-.043		-.046		-.051	-.053	-.069	-.069	-.092	-.093
	120	-.065		-.045		-.046		-.056	-.053	-.046	-.043	-.092	-.073
93.5	0	-.097	-.098	-.035	-.047	-.054	-.070	-.112	-.125	-.128	-.126	-.125	-.121
	120		-.138	-.035	-.053	-.056	-.070	-.100	-.111	-.105	-.110	-.139	-.134

[a]Data obtained from model symmetry conditions.

[redacted]

NACA

[redacted]

TABLE III.- PRESSURE-COEFFICIENT DATA (PRESENTED IN FIGS. 16 AND 17)

OVER UPPER SURFACE OF THE FUSELAGE AS A BODY OF REVOLUTION

Station (percent)	Radial angle ϕ	Angle of attack						
		-5	0	0	2	4	6	10
1.7	180	0.300	0.213	0.214	0.182	0.157	0.137	0.102
3.4		.324	.232	.231	.195	.168	.147	.105
5.9		.303	.220	.223	.185	.164	.145	.102
6.9		.287	.207	.207	.179	.159	.134	.086
8.5		.302	.217	.218	.182	.155	.129	.088
11.0		.213	.138	.136	-----	.089	.064	.033
16.8		.111	.041	.040	.016	0	-.010	-.042
19.9		.029	-.023	-.012	-.047	-.053	-.052	-.068
24.4		.007	-.031	-.031	-.045	-.052	-.055	-.052
27.3		.006	-.026	-.028	-.037	-.043	-.046	-.052
34.7		.020	-.015	-.013	-.023	-.023	-.025	-.016
38.7		.024	.001	0	-.007	-.008	-.006	-.002
44.8		.014	-.014	-.015	-.024	-.025	-.019	-.020
46.3		-.008	-.033	-.023	-.043	-.039	-.033	-.028
47.5		-.025	-.033	-.017	-.042	-.035	-.028	-.030
52.5		-.014	-.033	-.023	-.041	-.038	-.023	-.017
59.7		-.025	-.031	-.031	-.033	-.029	-.025	-.012
73.2		-.037	-.053	-.054	-.053	-.051	-.041	-.040
74.5		-.046	-.049	-.036	-.058	-.055	-.038	-.038
79.0		-.038	-.041	-.031	-.045	-.036	-.019	-.030
84.1		-.049	-.046	-.047	-.042	-.033	-.019	-.033
86.0		-.042	-.042	-.042	-.041	-.028	-.011	-.030
90.0		-.042	-.044	-.034	-.050	-.036	-.012	-.028
93.5		-.098	-.036	-.025	-.078	-.088	-.073	-.095
96.0		-.166	-.049	-.050	-.070	-.110	-.124	-.172

[redacted]

NACA

[redacted]

TABLE IV.- PRESSURE-COEFFICIENT DATA (PRESENTED IN FIG. 14) FOR THE FUSELAGE WITH CANOPIES

Station (percent)	Radial angle ϕ	Angle of attack					
		-5	0	2	4	6	10
5.6	0	0.131	0.197	0.223	0.266	0.303	0.381
	60	.156	.197	.209	.223	.234	.230
	90	.187	.197	.190	.190	.180	.130
	120	.238	.201	.178	.166	.148	.084
	180	.287	.201	.168	.150	.133	.082
10.9	0	.090	.152	.180	.217	.251	.330
	60	.106	.146	.155	.174	.186	.194
	90	-----	.154	.151	.156	.137	.100
	120	.226	.189	.178	.168	.139	.090
	180	.458	.352	.311	.280	.251	.198
22.0	0	-.075	-.044	-.027	.001	.020	.072
	60	-.059	-.028	-.015	.001	-.004	-.010
	120	-.067	-.059	-.053	-.044	-.054	-.074
	147	-.100	-.116	-.119	-.111	-.120	-.126
	180	-.104	-.150	-.156	-.142	-.162	-.186
34.6	0	-.030	-.007	.002	.021	.036	.078
	60	-.032	-.024	-.015	.001	-.010	-.026
	90	-.038	-.032	-.033	-.036	-.062	-.104
	120	-.026	-.024	-.029	-.036	-.066	-.120
	153	-.017	-.036	-.041	-.042	-.048	-.080
	180	-.019	-.036	-.041	-.030	-.034	-.024
46.2	90	-.065	-.056	-.053	-.056	-.088	-.160
	120	-.046	-.052	-.053	-.052	-.078	-.126
	158	.011	-.007	-.017	-.019	-.022	-.026
	180	.005	-.012	-.013	-.009	-.008	-.018
59.7	0	-.034	-.038	-.033	-.021	-.026	-.010
	0				-.032		
	90	-.046	-.020	-.025	-.025	-.056	-.110
	120	-.038	-.020	-.013	-.015	-.032	-.054
	158	-.026	-.028	-.033	-.025	-.022	-.026
	180	-.019	-.028	-.033	-.023	-.024	-.020
73.1	0	-.040	-.045	-.045	-.036	-.028	-.026
	60	-.059	-.048	-.053	-.052	-.060	-.102
	90	-.073	-.056	-.062	-.060	-.070	-.122
	120	-.067	-.052	-.058	-.054	-.058	-.082
	158	-.026	-.024	-.029	-.023	-.022	-.042
	180	-.011	-.016	-.021	-.013	-.008	-.010
84.3	0	-.034	-.052	-.058	-.052	-.060	-.102
	60	-.059	-.052	-.053	-.050	-.068	-.106
	90	-.067	-.048	-.053	-.052	-.064	-.102
	120	-.071	-.048	-.053	-.052	-.054	-.078
93.5	0	-.069	-.073	-.074	-.066	-.072	-.110
	120	-.141	-.114	-.113	-.105	-.025	-.108

[redacted]

TABLE V.— SUPPLEMENTARY PRESSURE-COEFFICIENT DATA

FOR THE FUSELAGE AS A BODY OF REVOLUTION

Station (percent)	Radial angle ϕ	Angle of attack					
		-3	-3	-2	-2	8	8
5.6	0	0.155		0.170	0.174		0.345
	60	.171		.185	.180		.251
	90	.187		.197	.195		.174
	120	.220		.217	.215		.125
	180	.249		.236	-----		-----
10.9	0	.110		.125	.128		.290
	60	.124		-----	.132		.190
	90	-----		-----	.152		.123
	120	.175		.174	.178		.080
	180	.179		.172	.170		.049
22.0	0	-.074		-.065	-.059		.031
	60	-.072		-.063	-.059		-.036
	120	-.052		-.049	-.046		-.104
	147	-.038		-.039	-.042		-.102
	180	-.032		-.037	-----		-----
34.6	0	-.025		-.020	-.017		.039
	60	-.025		-.018	-.015		-.030
	90	-.023		-.016	-.017		-.065
	120	-.017		-.012	-.007		-.057
	153	-.009		-.010	-.005		-.038
	180	.009		0	0		-.018
46.2	0						
	90	-.054		-.045	-.044		-.095
	120	-.046		-.037	-.040		-.075
	158	-.040		-.037	-----		-.034
	180	-.042		-.041	-----		-.034
59.7	0	-.030		-.028	-----		-.010
	90	-.034		-.026	-.025		-.075
	120	-.030		-.028	-.029		-.067
	158	-.036		-.033	-.032		-.026
	180	-.034		-.028	-.029		-.018
73.1	0	-.058		-.053	-.050		-.038
	60	-.058		-.055	-.056		-.087
	90	-.064		-.057	-.059		-.104
	120	-.062		-.053	-.059		-.075
	158	-.054		-.051	-.050		-.049
	180	-.054		-.053	-.050		-.038
84.3	0	-.034		-.035	-.034		-.042
	60	-.050		-.041	-.042		-.083
	90	-.050		-.043	-.048		-.083
	120	-.050		-.045	-.046		-.059
93.5	0	-.097		-.063	-.079		-.128
	120	-.083		-.057	-.075		-.124

[redacted]

NACA

CONFIDENTIAL

TABLE VI.- SUPPLEMENTARY PRESSURE-COEFFICIENT DATA

OVER THE UPPER SURFACE OF THE FUSELAGE

AS A BODY OF REVOLUTION

Station (percent)	Radial angle ϕ	Angle of attack	
		-2	8
1.7	180	0.251	0.119
3.4		.268	.128
5.9		.259	.125
6.9		.239	.110
8.5		.253	.104
11.0		.170	.049
16.8		.068	-.025
19.9		.009	-.063
24.4		-.014	-.062
27.3		-.014	-.052
34.7		0	-.018
38.7		.009	-.002
44.8		-.004	-.018

Station (percent)	Radial angle ϕ	Angle of attack	
		-2	8
46.3	180	0.002	-0.034
47.5		-.012	-.034
52.5		-.017	-.023
59.7		-.029	-.018
73.2		-.050	-.038
74.5		-.035	-.041
79.0		-.030	-.025
84.1		-.047	-.026
86.0		-.040	-.020
90.0		-.034	-.021
93.5		-.050	-.087
96.0		-.066	-.140

CONFIDENTIAL

[redacted]

TABLE VII.— SUPPLEMENTARY PRESSURE-COEFFICIENT DATA

FOR THE FUSELAGE WITH CANOPIES

Station (percent)	Radial angle ø	Angle of attack		
		-3	-2	8
5.6	0	0.151	0.165	0.342
	60	.171	.181	.232
	90	.189	.193	.156
	120	.222	.213	.117
	180	.249	.229	.105
10.9	0	.110	.122	.289
	60	.130	.132	.187
	90	-----	-----	.117
	120	.212	.201	.109
	180	.414	.396	.219
22.0	0	-.066	-.061	.042
	60	-.045	-.042	-.013
	120	-.062	-.063	-.068
	147	-.106	-.111	-.127
	180	-.127	-.136	-.180
34.6	0	-.023	-.020	.052
	60	-.031	-.028	-.021
	90	-.031	-.030	-.088
	120	-.027	-.022	-.099
	153	-.027	-.030	-.066
	180	-.026	-.034	-.035
46.2	90	-.059	-.058	-.127
	120	-.045	-.050	-.113
	158	.002	-.010	-.029
	180	-.006	-.010	-.017
59.7	0	-.039	-.042	-.023
	90	-.031	-.028	-.078
	120	-.033	-.026	-.048
	158	-.025	-.026	-.025
	180	-.023	-.026	-.023
73.1	0	-.045	-.046	-.033
	60	-.053	-.050	-.080
	90	-.062	-.058	-.101
	120	-.057	-.054	-.074
	158	-.025	-.026	-.033
	180	-.017	-.018	-.013
84.3	0	-.041	-.046	-.066
	60	-.055	-.054	-.088
	90	-.057	-.052	-.088
	120	-.057	-.054	-.070
93.5	0	-.070	-.073	-.074
	120	-.127	-.119	-.105

[redacted]

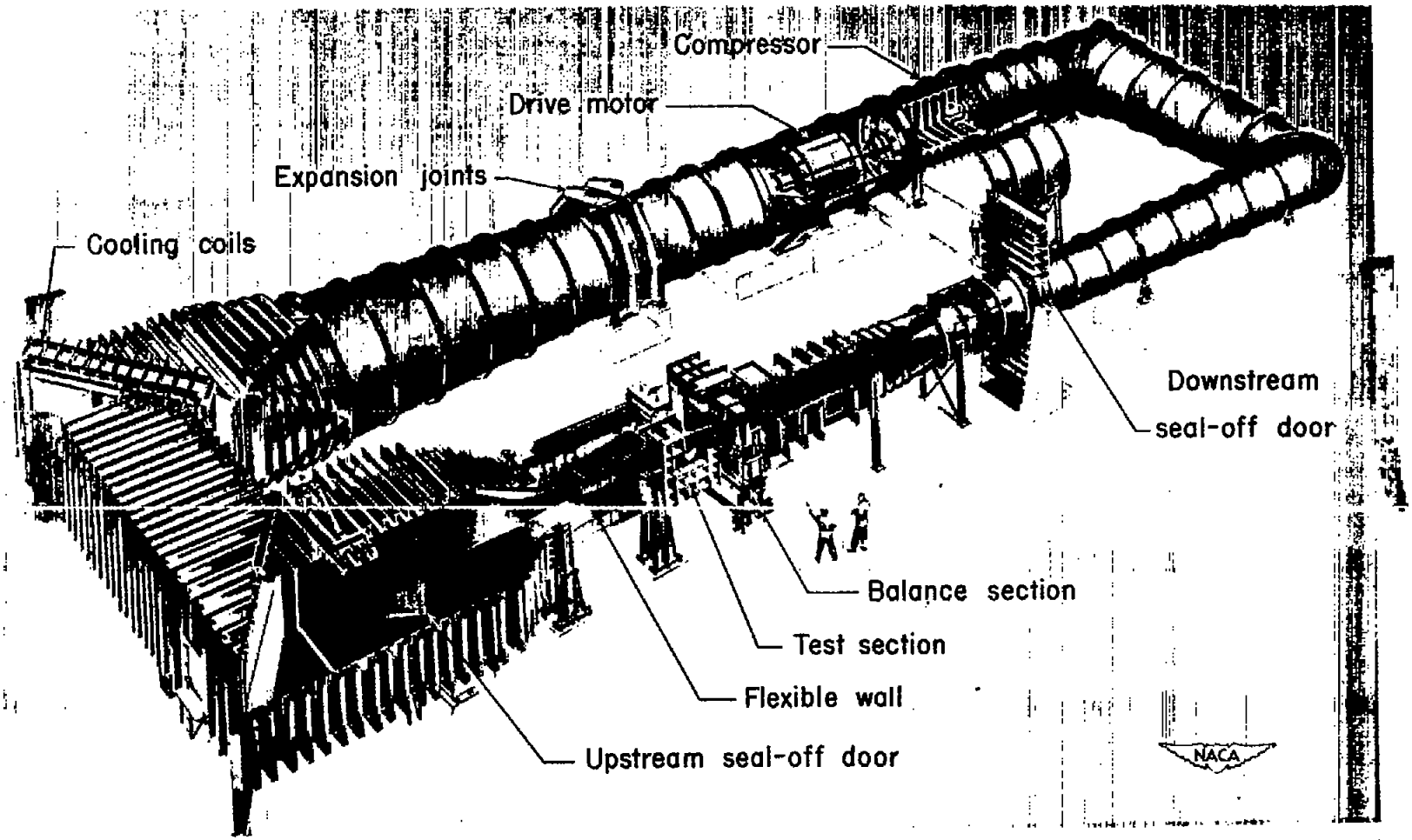

Figure 1.- Pictorial drawing of the Langley 4- by 4-foot supersonic tunnel.

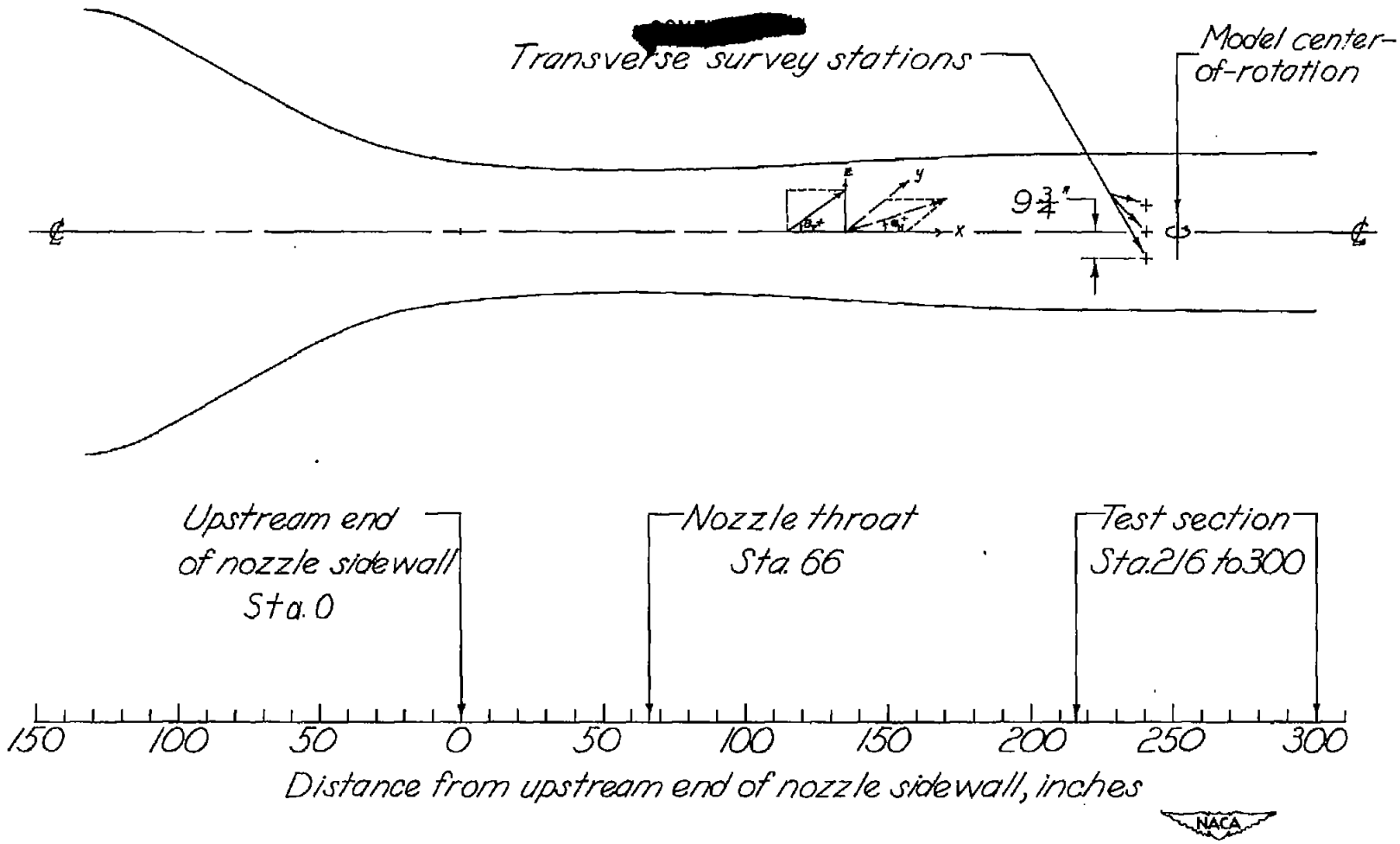

Figure 2.- Schematic layout of entrance cone, nozzle, and test section of the Langley 4-by 4-foot supersonic tunnel.

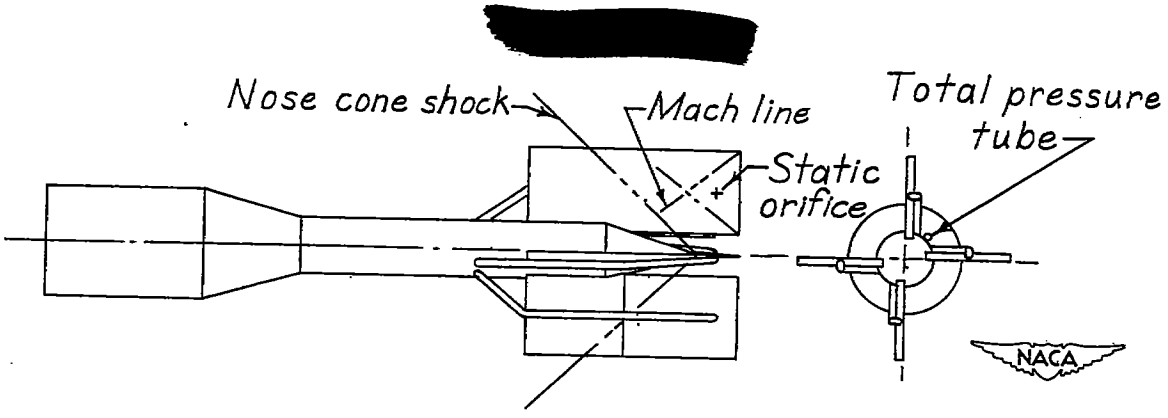

(a) Schematic drawing of cruciform probe.

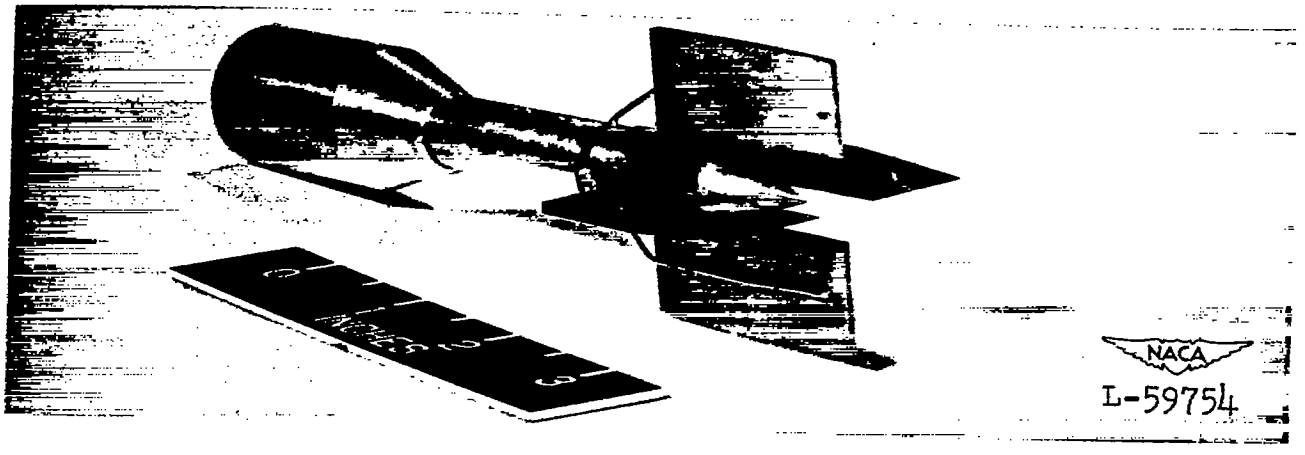

(b) Three-quarter-front view of cruciform probe.

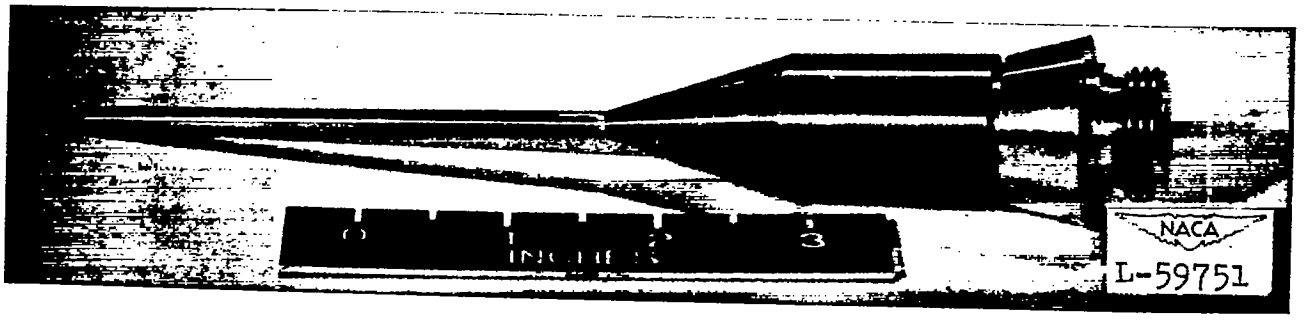

(c) Pitot-static probe.

Figure 3.- Calibration probes.

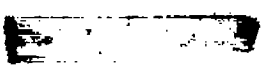

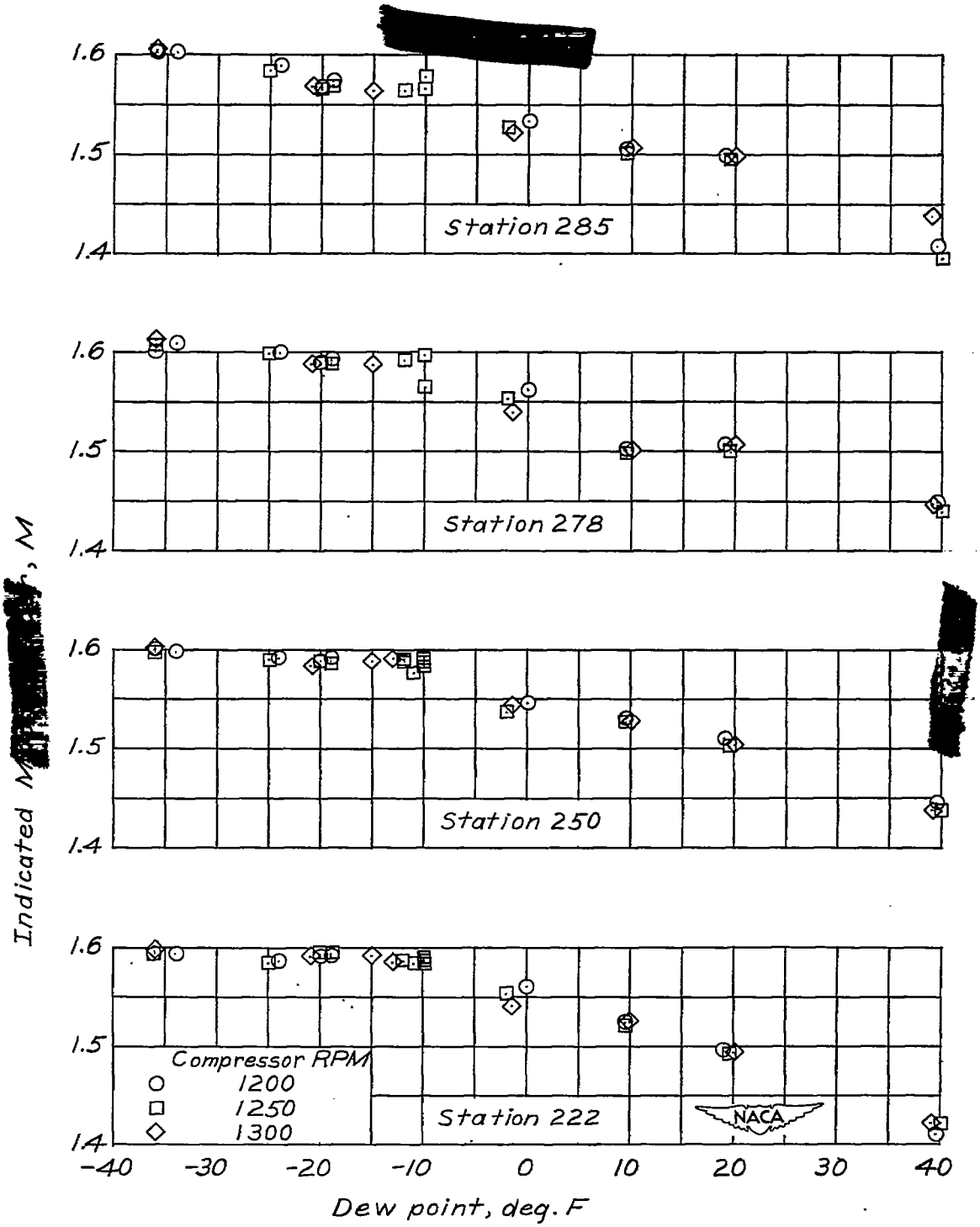

Figure 4.- Variation of local Mach number with dew point for representative stations along the nozzle axis of the Langley 4-by 4-foot supersonic tunnel for stagnation conditions of 110 degrees F and 0.25 atmospheres.

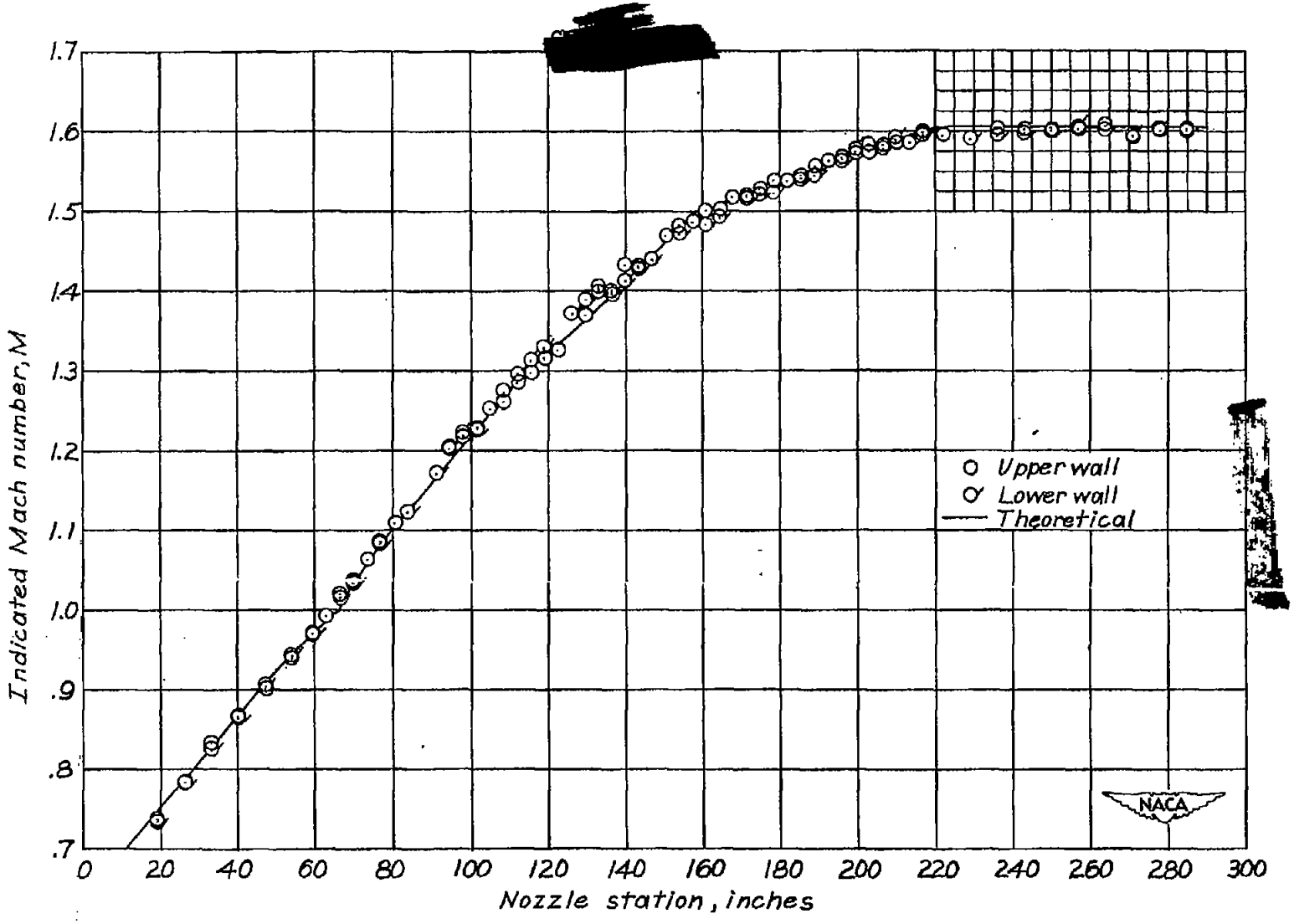

Figure 5.- Mach number distribution along nozzle walls of the Langley 4-by 4-foot supersonic tunnel.

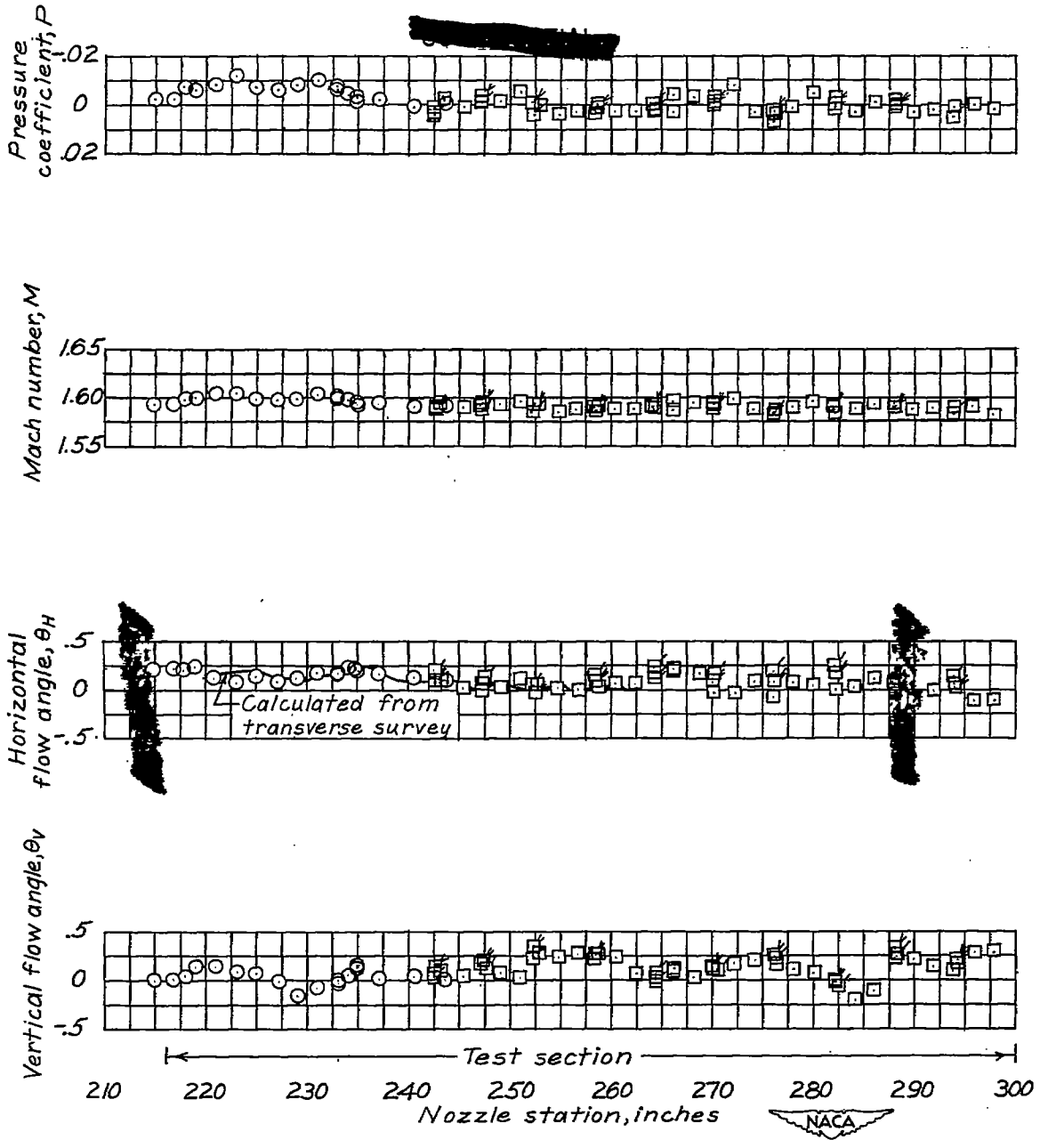

Figure 6.- Longitudinal flow parameters along the test section axis of the Langley 4- by 4-foot supersonic tunnel.

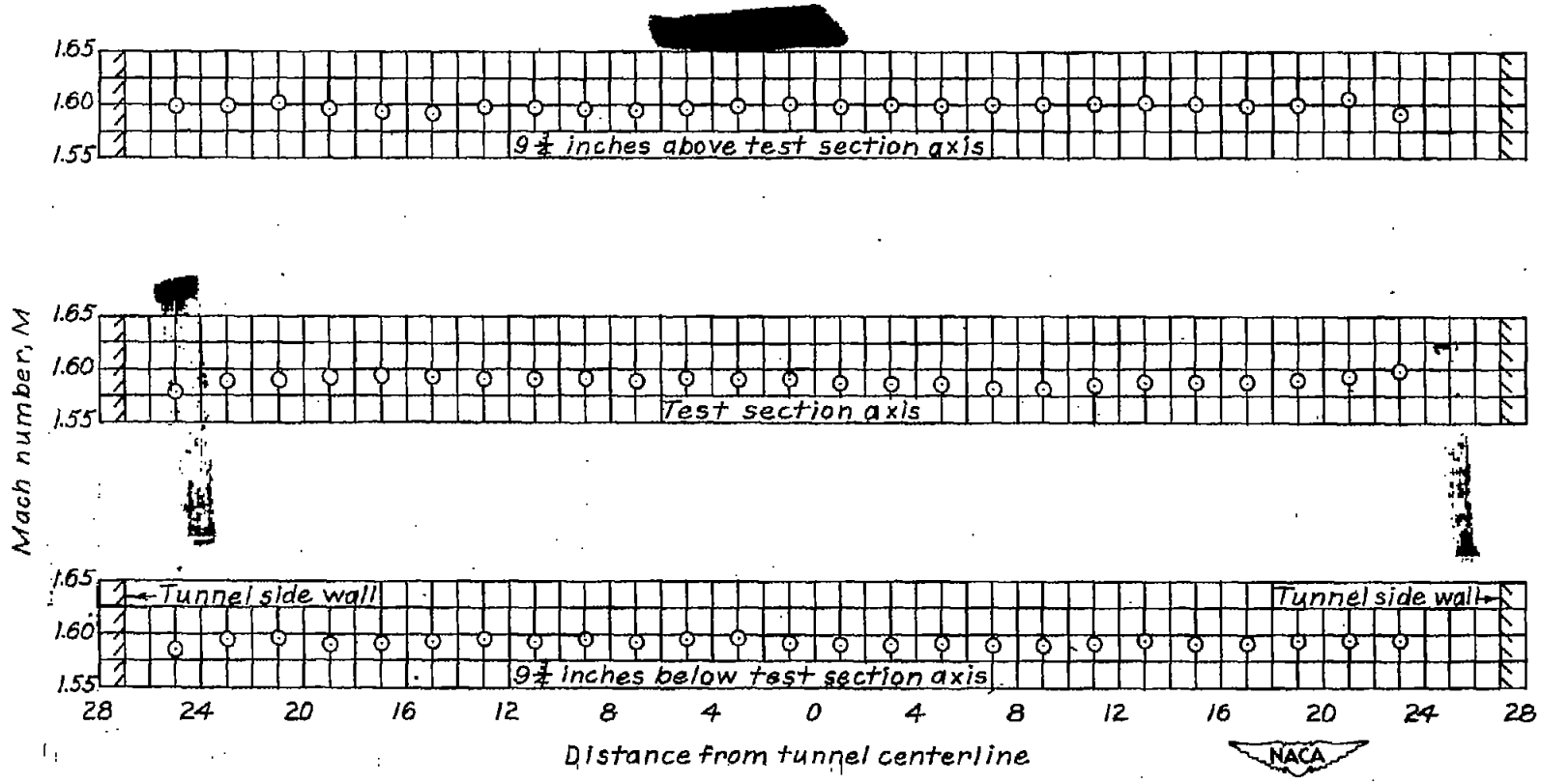

Figure 7.- Transverse Mach number distribution at station 241 in the test section of the Langley 4-by 4-foot supersonic tunnel. Up[illegible] view.

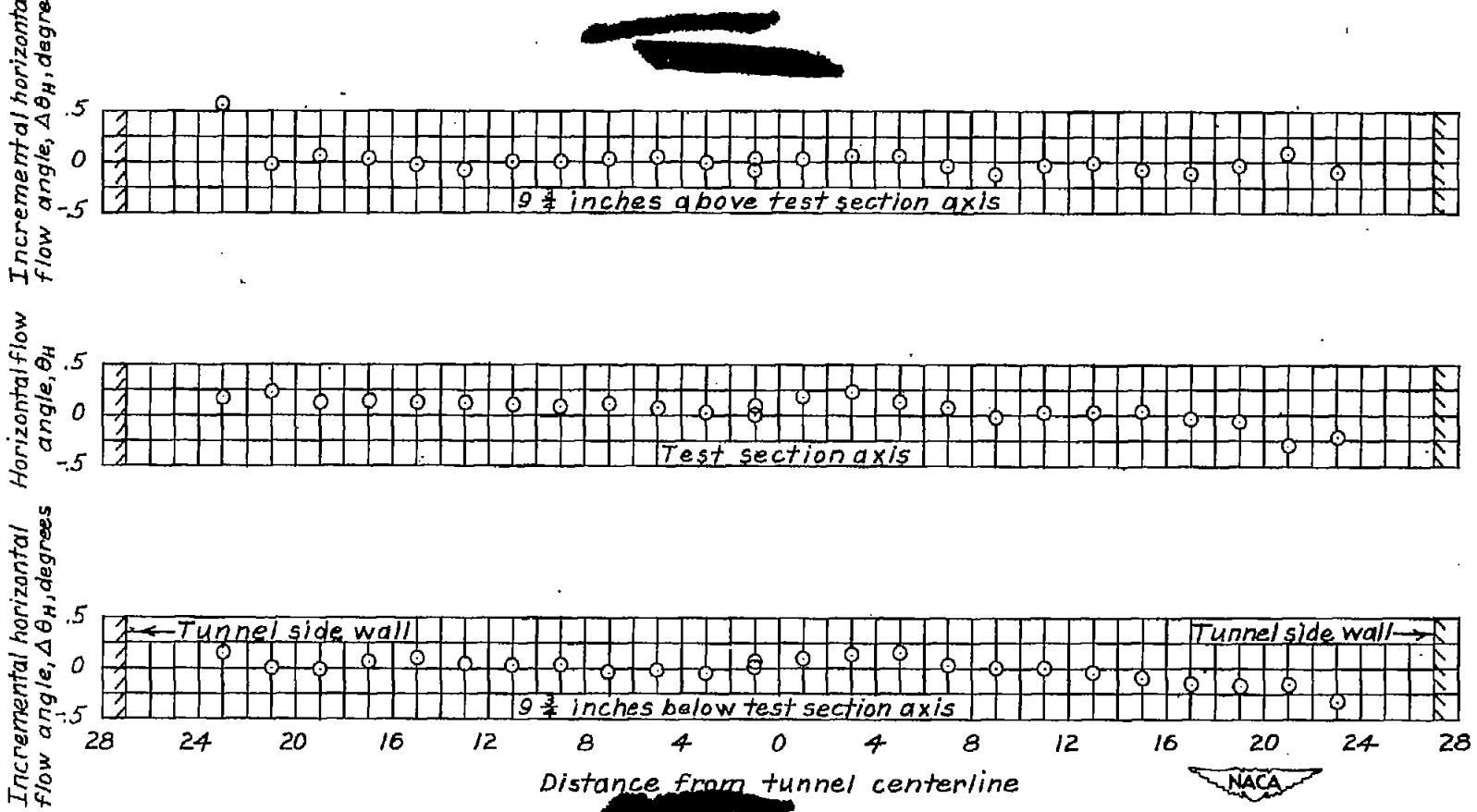

Figure 8.- Horizontal flow angles, in a transverse direction, at station 241 in the test section of the Langley 4-by 4-foot supersonic tunnel. Upstream view.

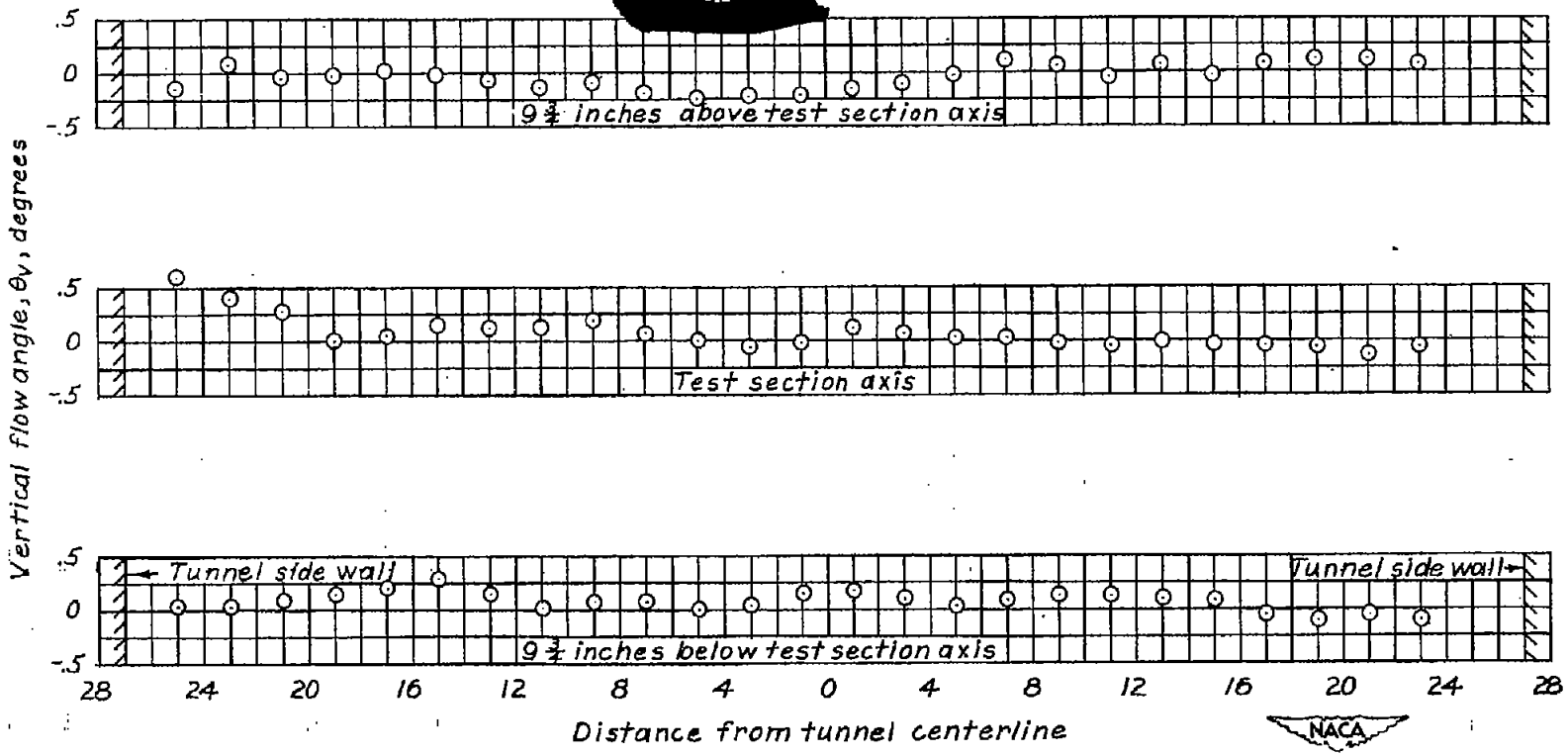

Figure 9.- Vertical flow angles, in a transverse direction, at station 241 in the test section of the Langley 4-by 4-foot super[redacted] Upstream view.

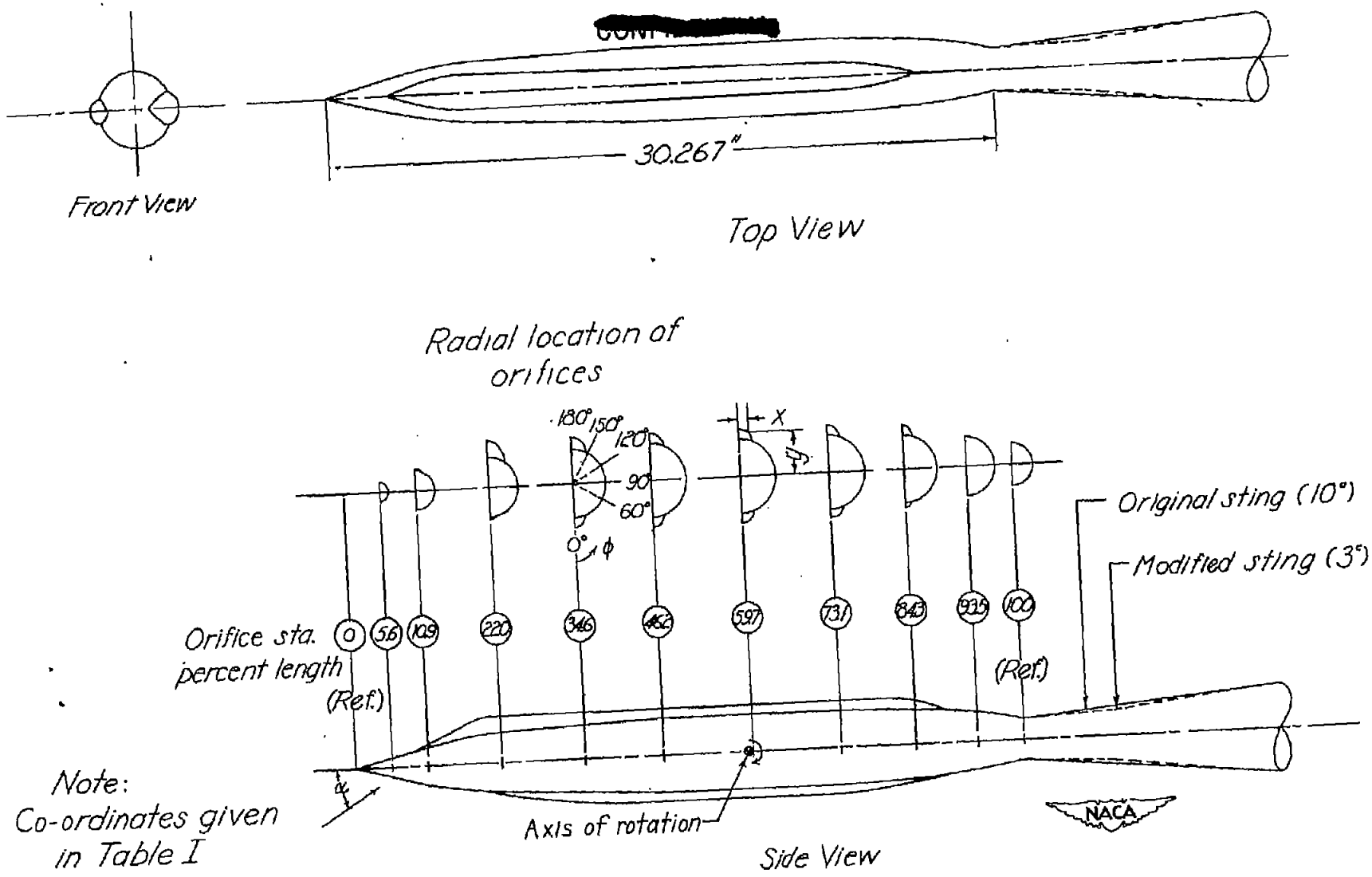

Figure 10.- Fuselage model layout.

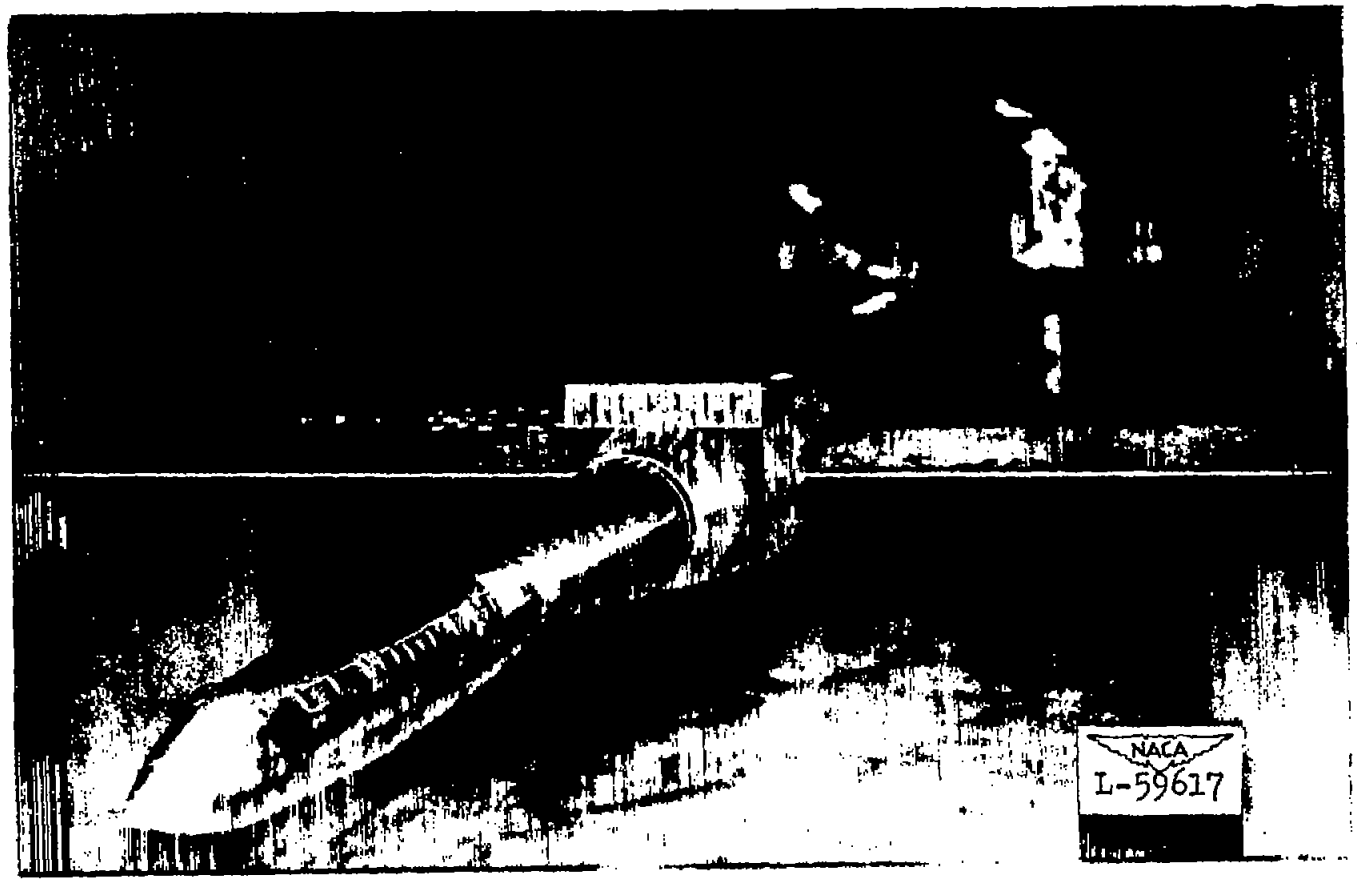

Figure 11.- Downstream view of the body of revolution in the Langley 4- by 4-foot supersonic tunnel.

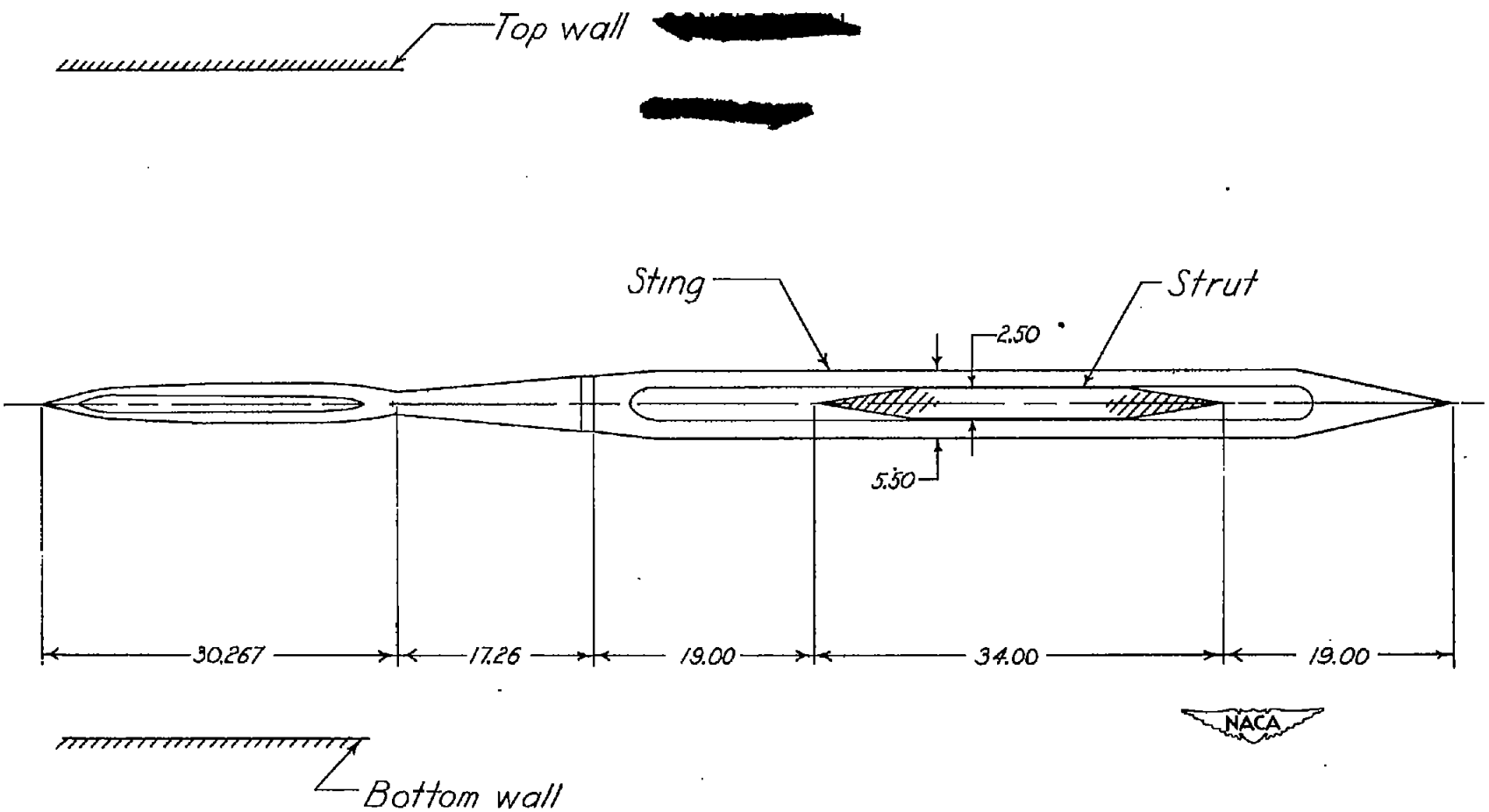

All dimensions in inches

Figure 12- Model and support installation.

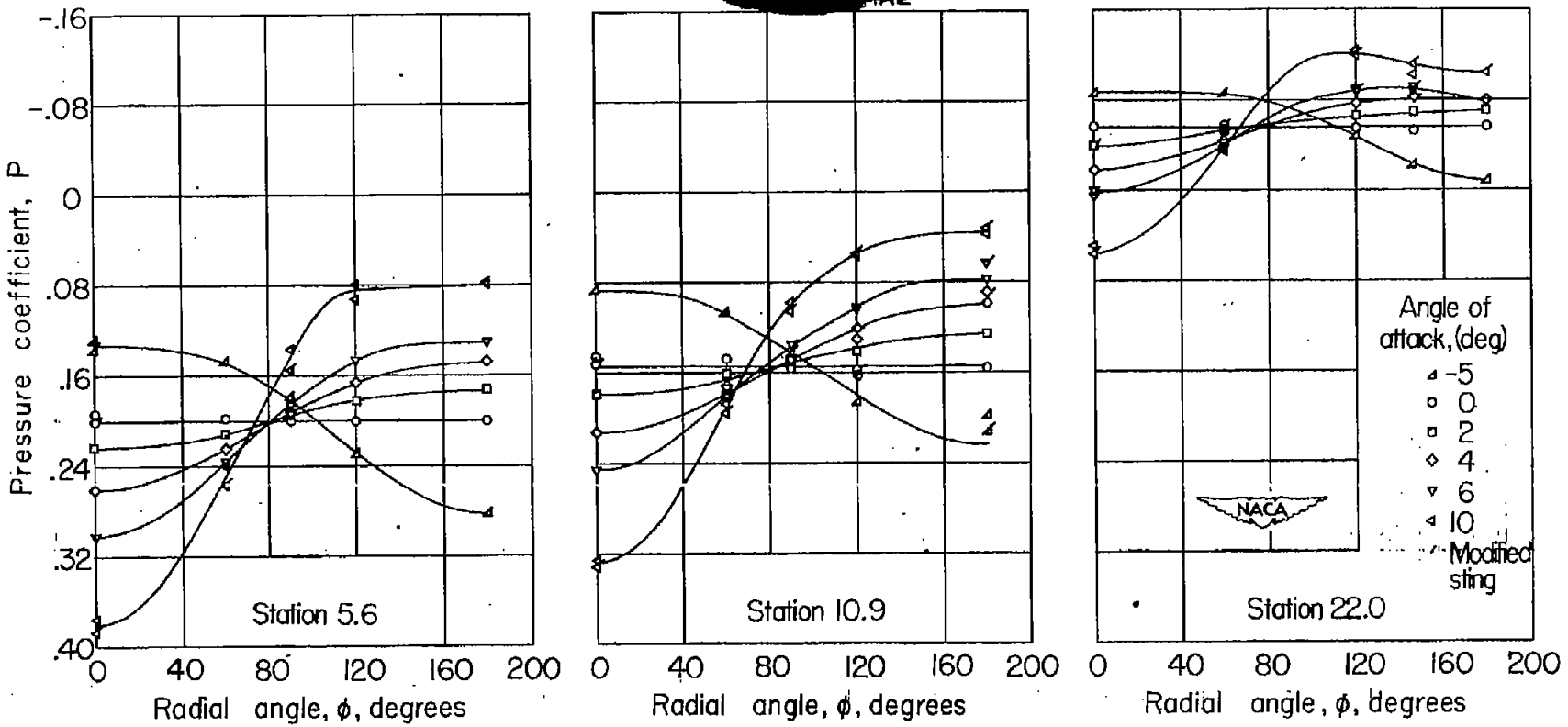

Figure 13a.—Pressure coefficient variation with radial position for nine representative stations for the fuselage as a body of revolution.

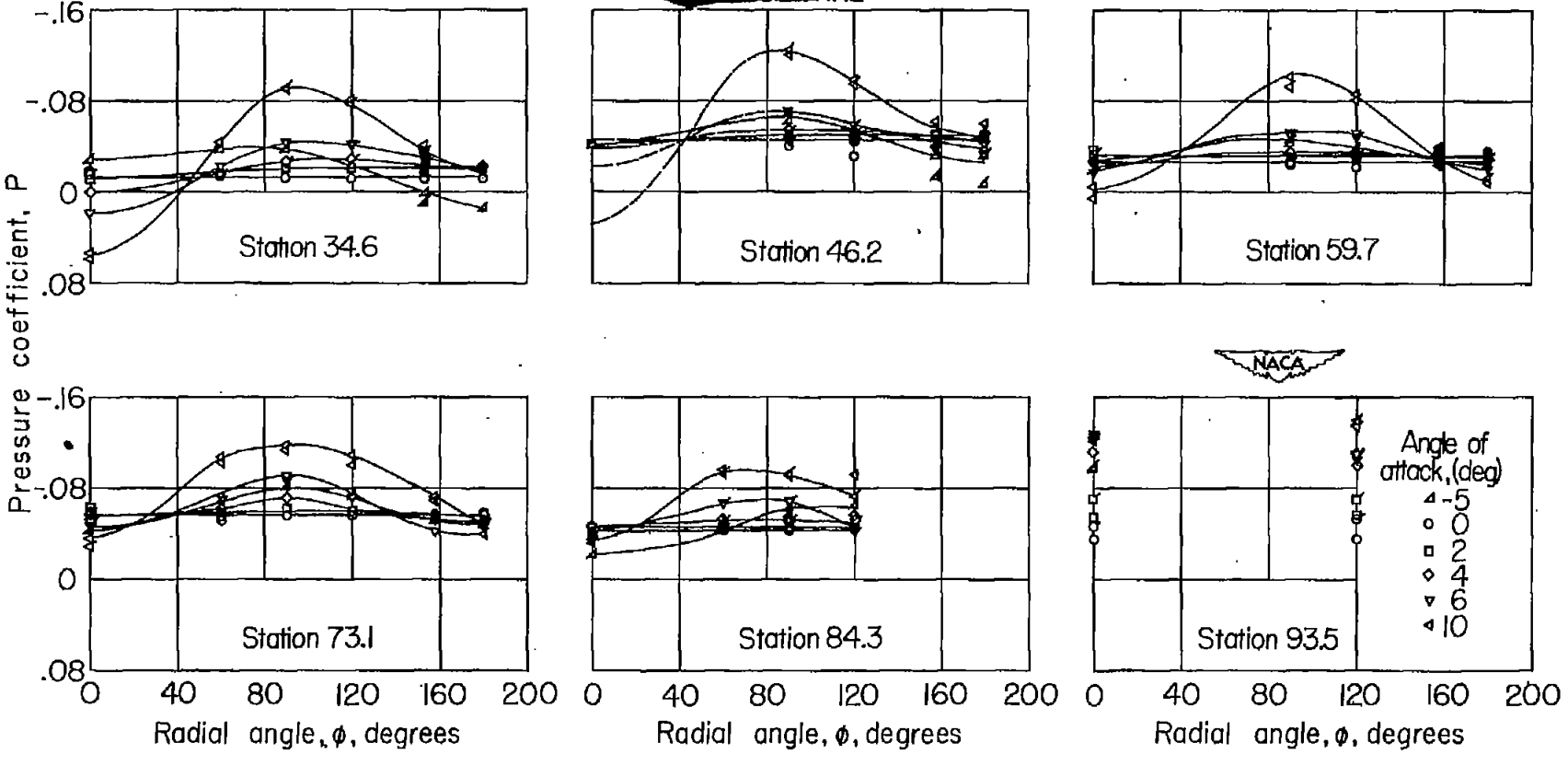

Figure 13 b.— Concluded.

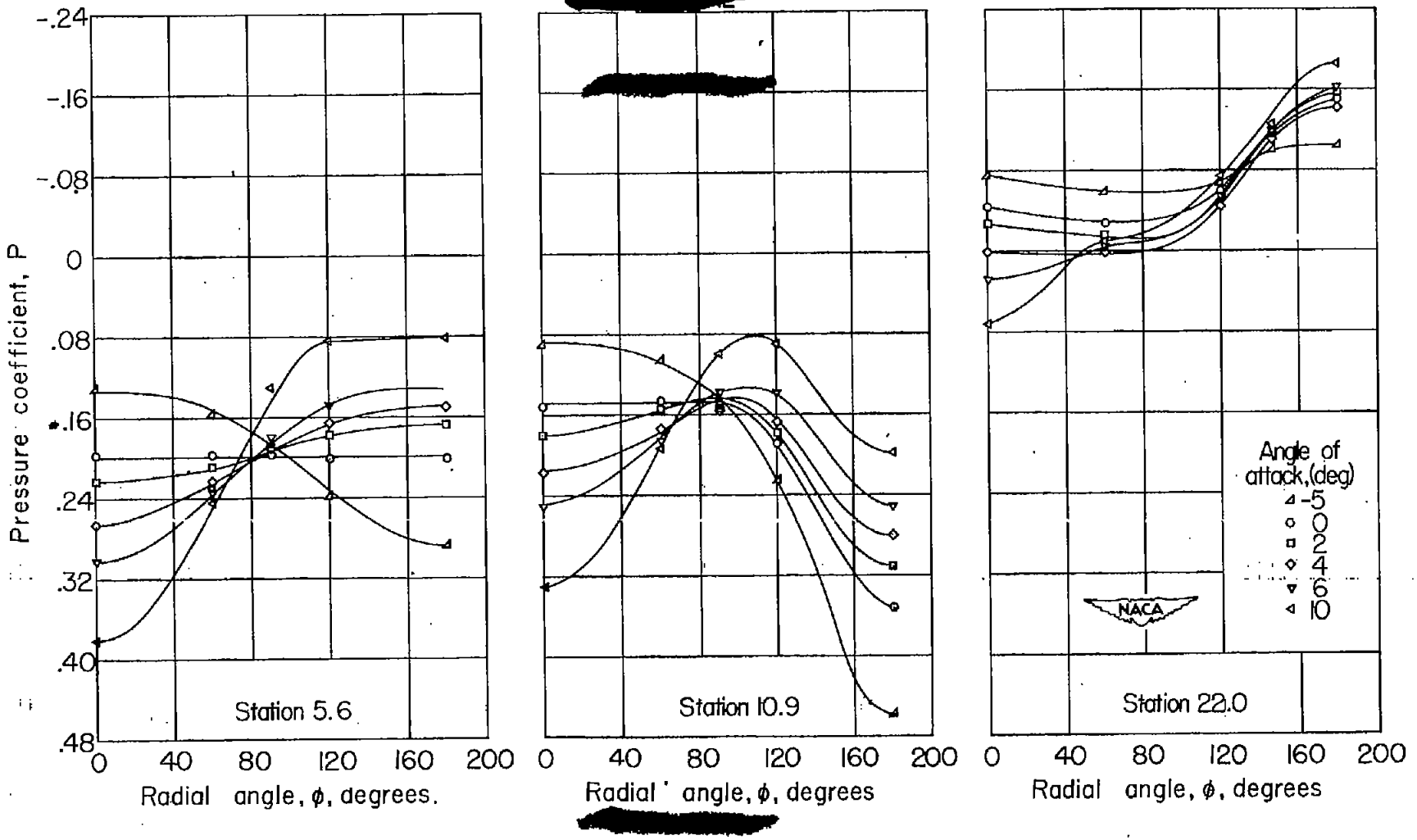

Figure 14 a — Pressure coefficient variation with radial position for nine representative stations for the fuselage with canopies.

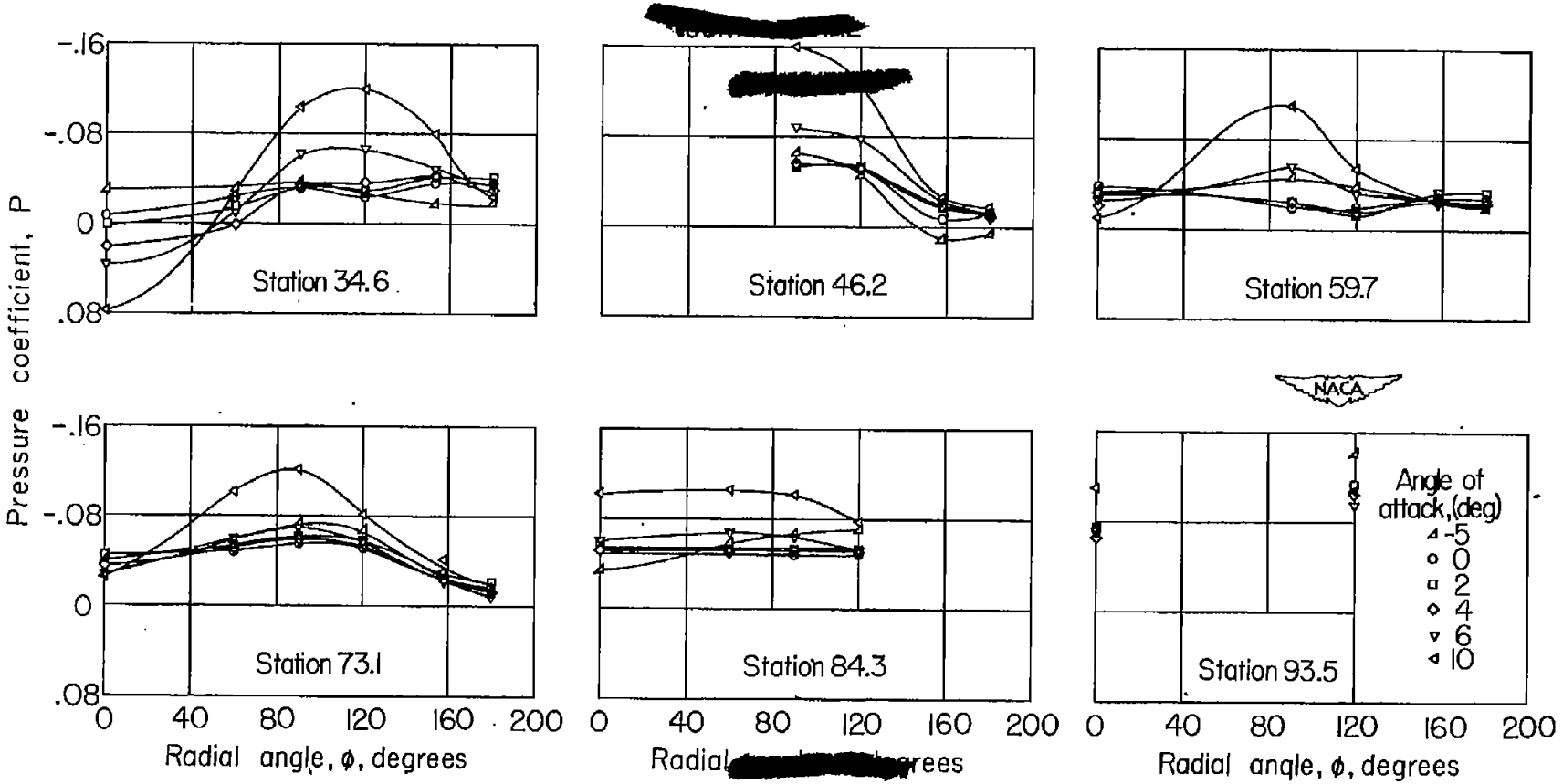

Figure 14 b.— Concluded.

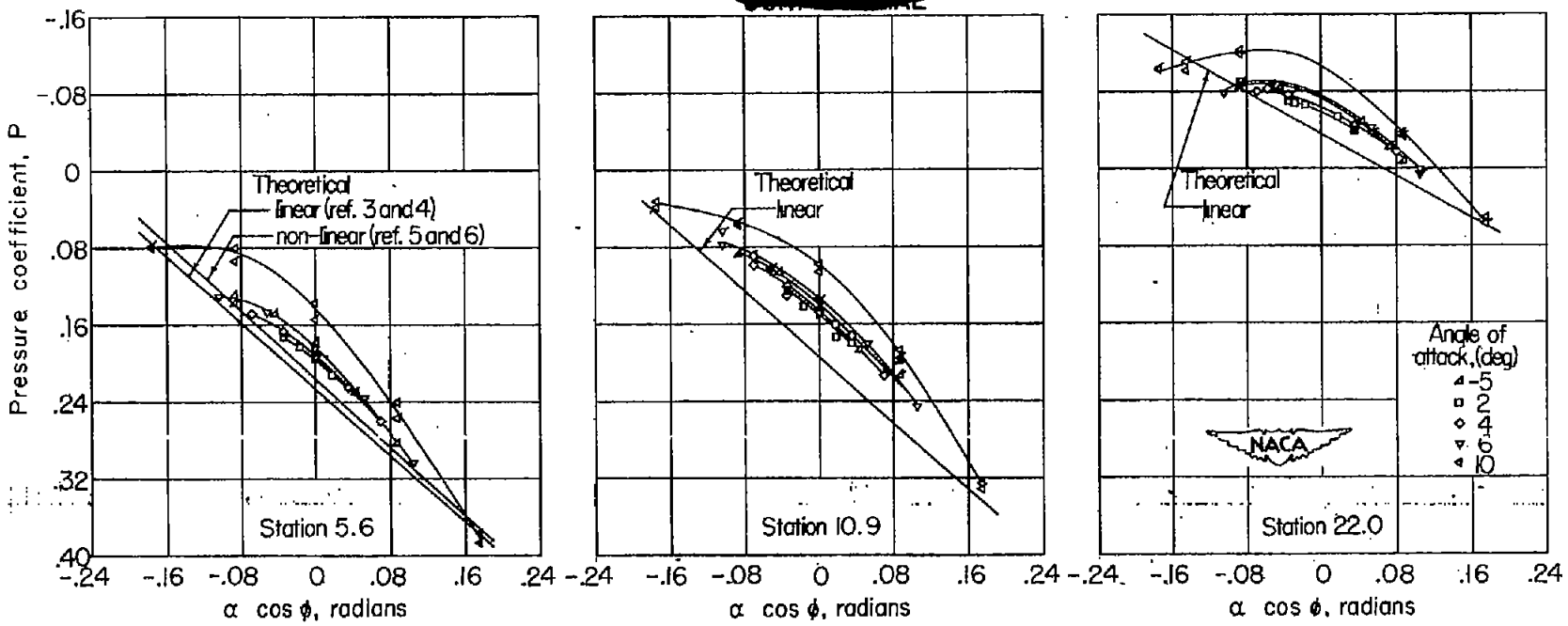

Figure 15a.—Experimental and theoretical pressure coefficient variations with $\alpha \cos \phi$ for nine representative stations for the fuselage as a body of revolution.

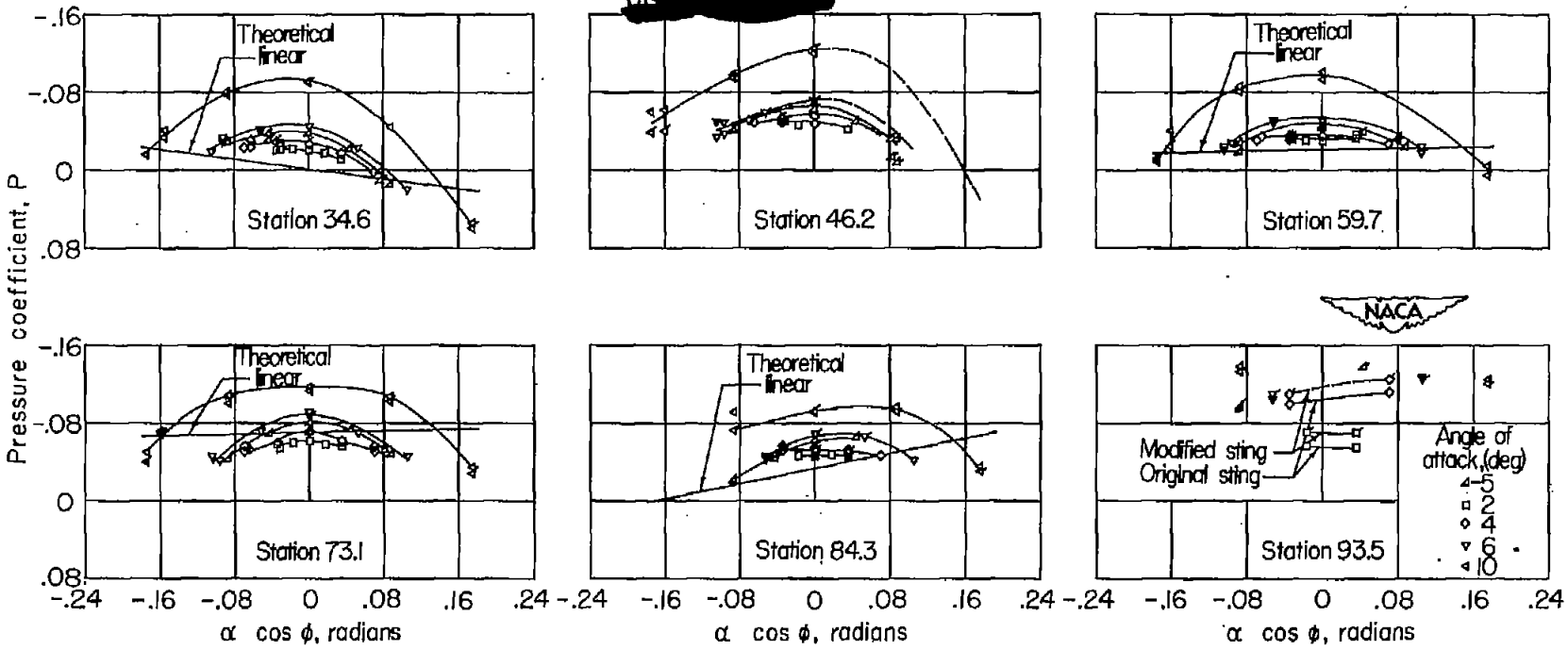

Figure 15 b.— Concluded.

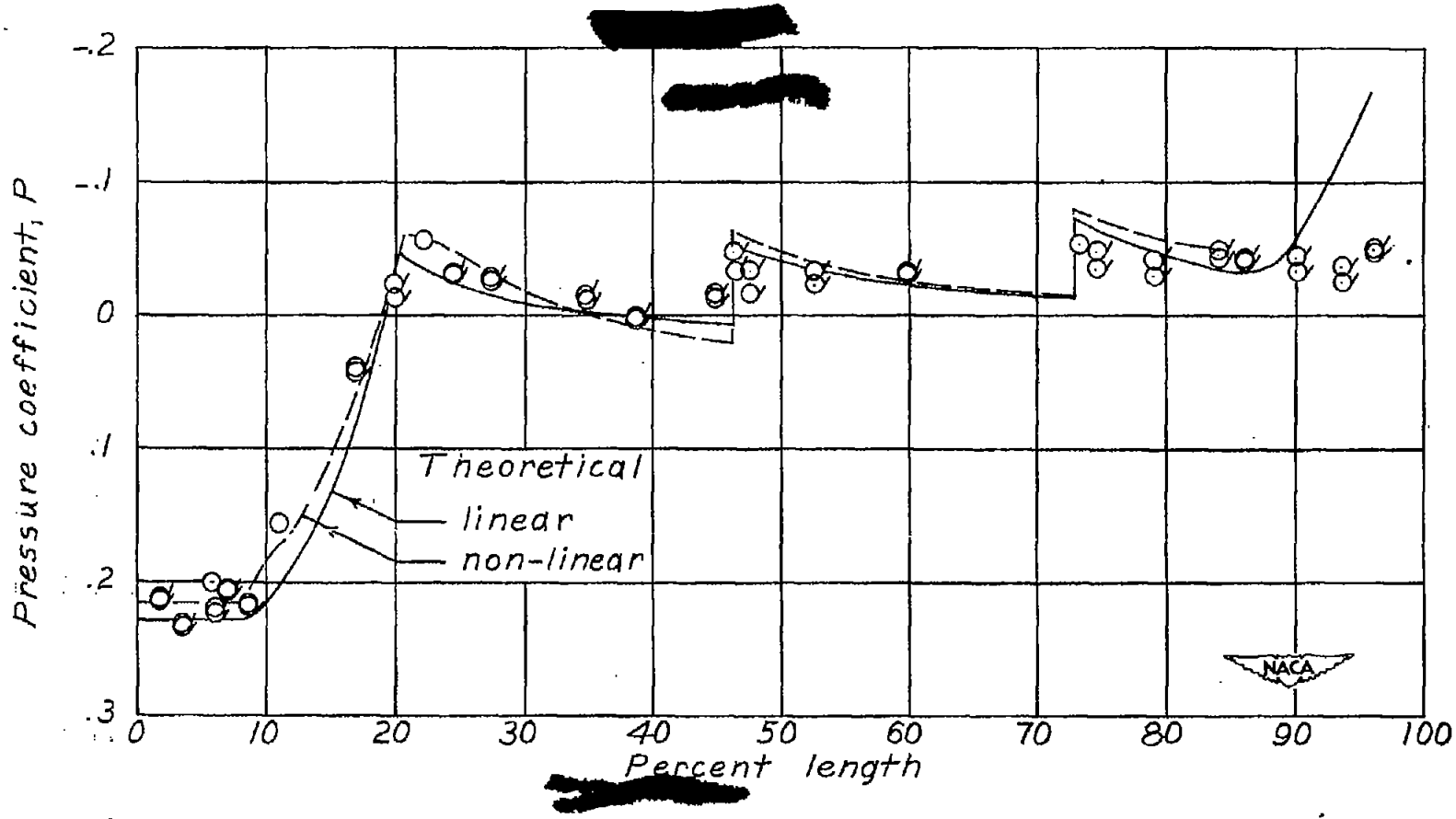

Figure 16.- Experimental and theoretical pressures over the body of revolution, for an angle of attack of zero degrees. $M = 1.59$.

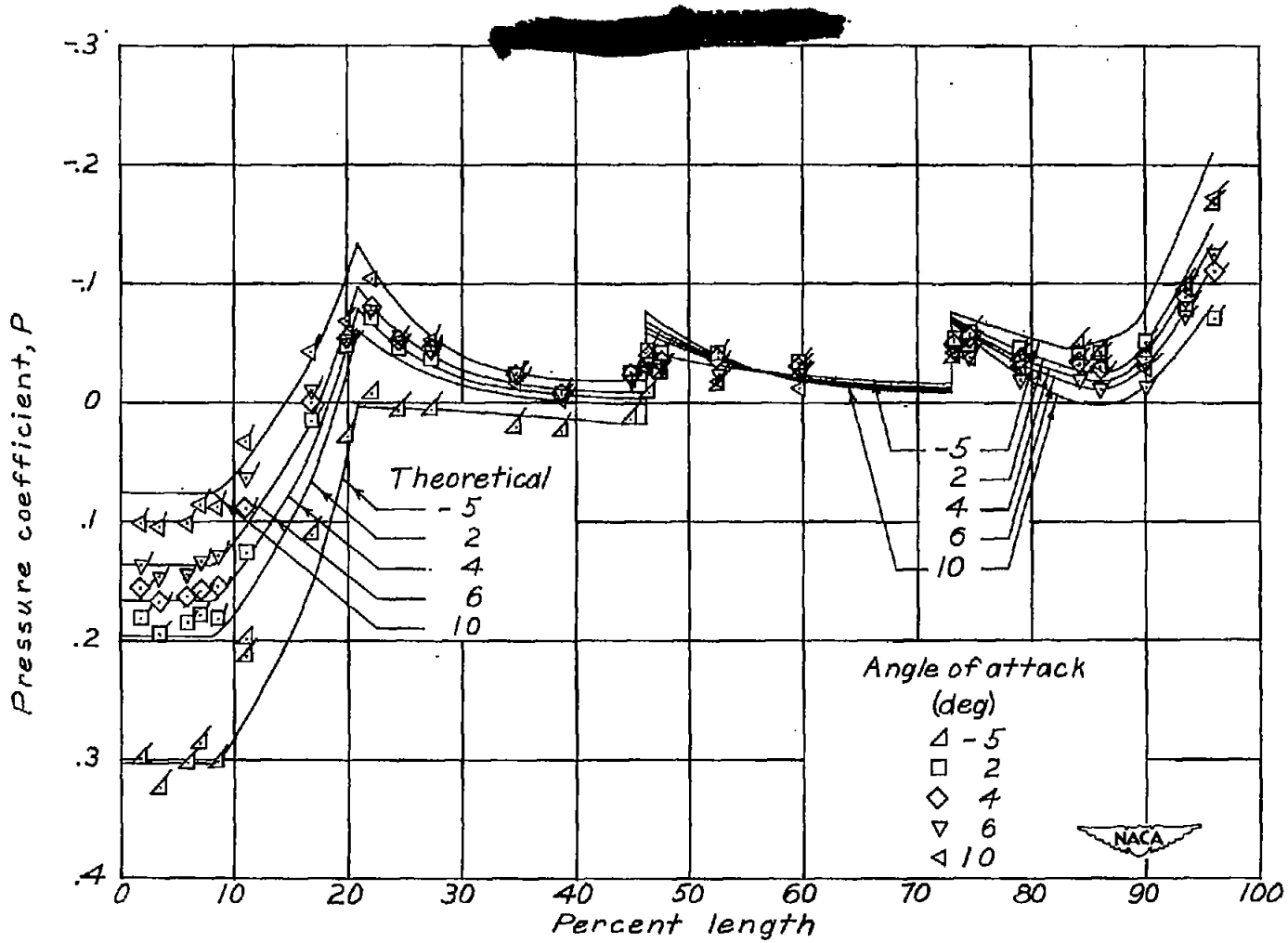

Figure 17.- Experimental and theoretical pressures over the upper surface ($\phi = 180°$) of the body of revolution for representative angles of attack. $M = 1.59$.

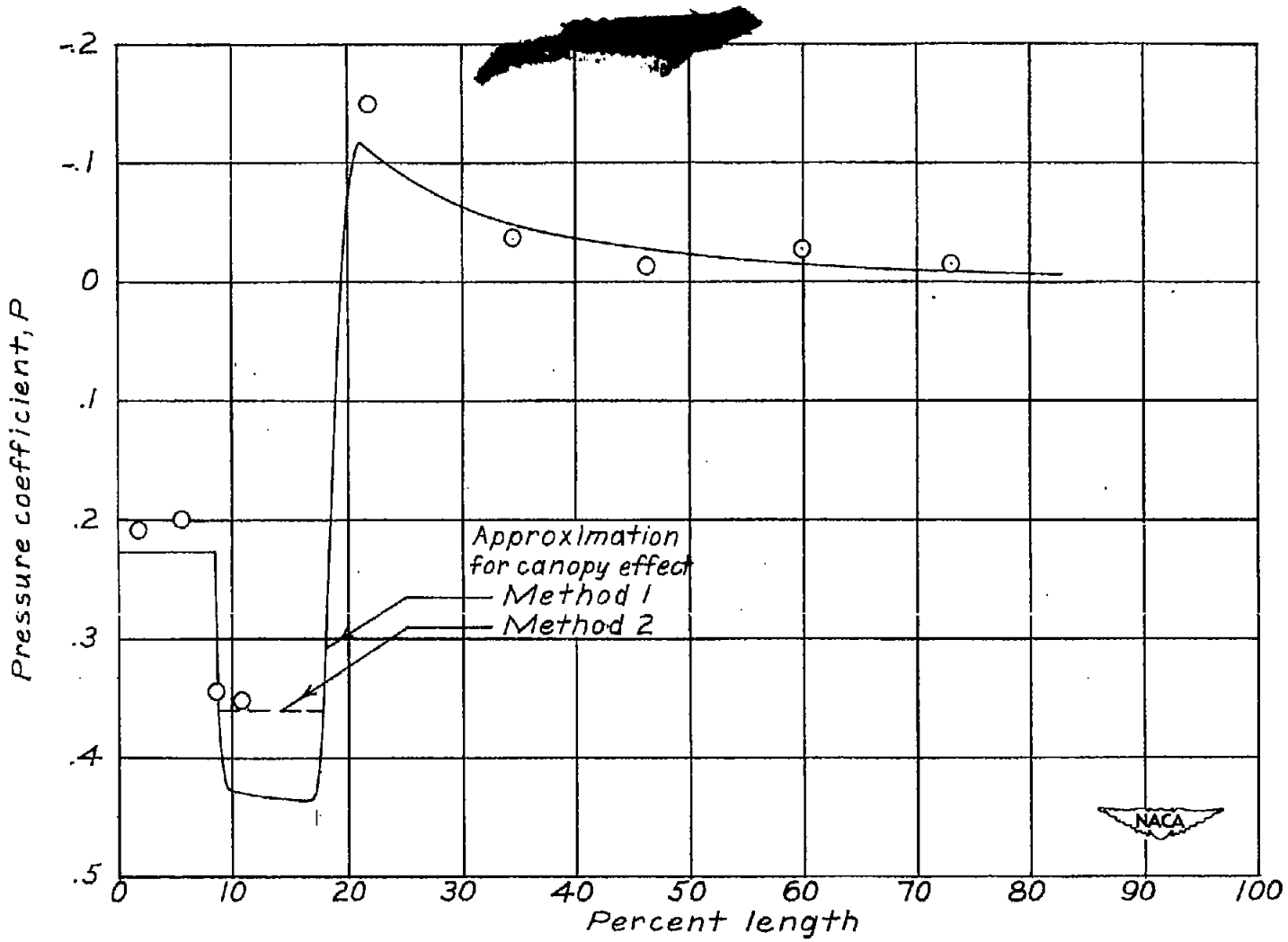

Figure 18.- Experimental and estimated pressures over the fuselage with canopies, $\phi = 180°$ [redacted] angle of attack of zero degrees. $M = 1.59$.

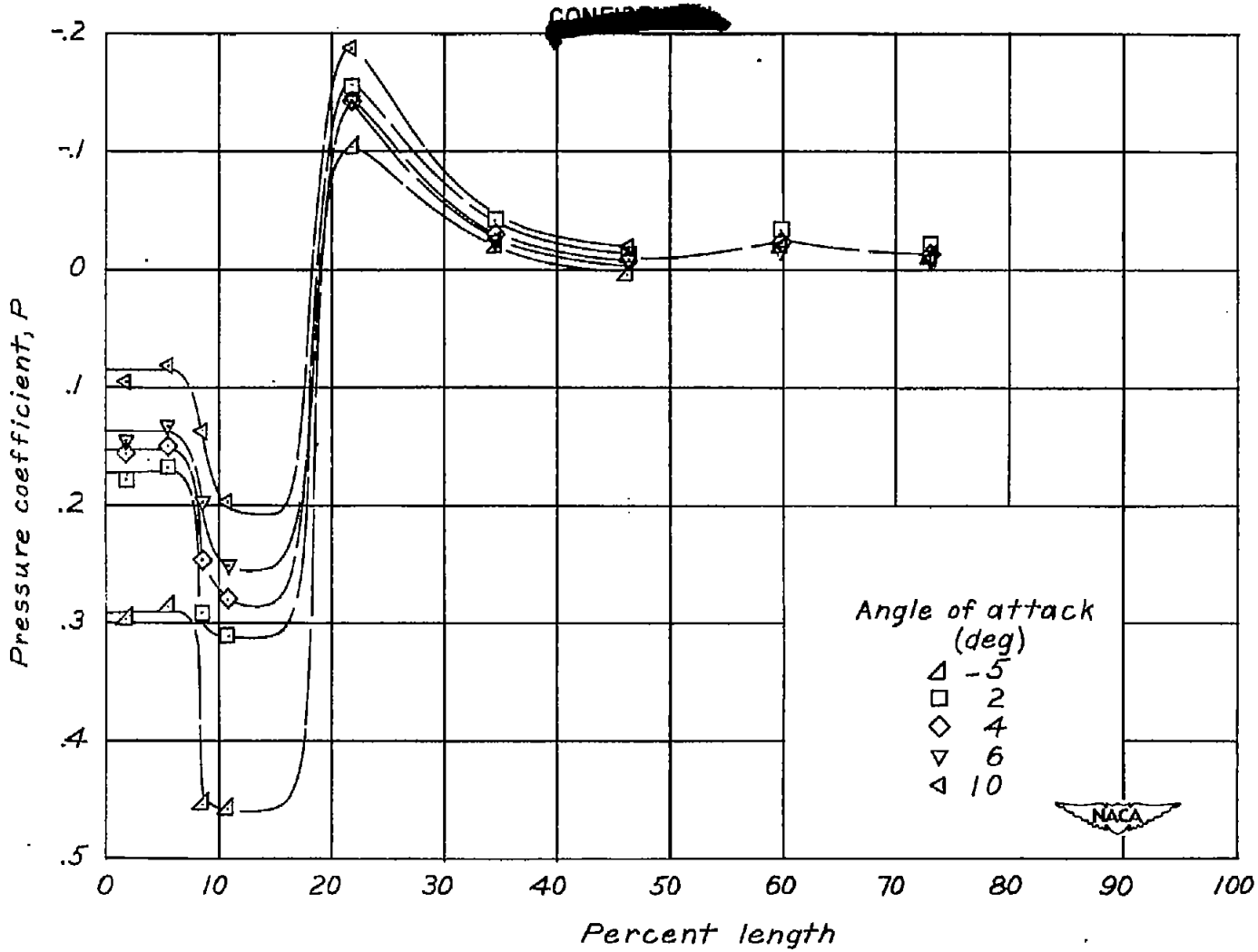

Figure 19.- Longitudinal pressure distribution over the upper surface of the fuselage with canopies for representative angles of attack. M=1.59.